UC Davis
San Francisco Estuary and Watershed Science

Title
The Effects of Hydrodynamic and Environmental Conditions on Juvenile Chinook Salmon Movements in the South Sacramento—San Joaquin Delta

Permalink
https://escholarship.org/uc/item/7f40x52h

Journal
San Francisco Estuary and Watershed Science, 24(3)

Authors
Gonsalves, Sydney
Buchanan, Rebecca
Bever, Aaron J.
et al.

Publication Date
2026-09-28

Supplemental Material
https://escholarship.org/uc/item/7f40x52h#supplemental

Copyright Information
This work is made available under the terms of a Creative Commons Attribution License, available at https://creativecommons.org/licenses/by/4.0/

Peer reviewed

eScholarship.org Powered by the California Digital Library
University of California

SAN FRANCISCO ESTUARY & WATERSHED SCIENCE
Sponsored by the Delta Stewardship Council and UC Davis Institute of the Environment

RESEARCH

The Effects of Hydrodynamic and Environmental Conditions on Juvenile Chinook Salmon Movements in the South Sacramento–San Joaquin Delta

Sydney M. Gonsalves*[1], Rebecca A. Buchanan[2], Aaron J. Bever[1], Michael L. MacWilliams[3], John W. Ferguson[1]

ABSTRACT

San Joaquin River-origin Central Valley Chinook Salmon are a species of conservation concern because they play an essential role in the health and function of California's aquatic ecosystems yet experience low survival as juveniles pass through the Sacramento–San Joaquin Delta (Delta) on their way to the Pacific Ocean. We analyzed 8 years of juvenile Chinook Salmon acoustic telemetry data near the State Water Project and Central Valley Project in the South Delta to inform how hydrodynamic and environmental conditions affect fish movement. The behavior of Chinook Salmon in this area was related to simulated outputs from a high-resolution hydrodynamic model that used a continuous-time multi-state Markov model. A total of 839 fish were detected near the facilities, and the median time fish spent in the area was 33 hours. Flow conditions near the water projects strongly influenced juvenile Chinook Salmon movement patterns. For fish detected at the Central Valley Project trash racks and outside the radial gates to Clifton Court Forebay at the State Water Project, the strongest effects on movement were from upstream-directed net flow, time of day, and turbidity. Export operations drew fish movement into the water export facilities when exports were high and at night. Movements in West Canal between Highway 4 and the radial gates were influenced by tidal flow and net flow. Fish primarily moved downstream on the ebb tide, especially when exports were lower. Study fish near the water projects experienced high predation, which reduced sample size and increased uncertainty. Our study identified factors that drive juvenile Chinook Salmon movements near the water projects and can be used to inform water operations and management decision-making that may improve salmon survival in the Delta.

KEY WORDS

Chinook Salmon, juvenile salmon, migration, multi-state model, acoustic telemetry, animal movement

SFEWS Volume 24 | Issue 3 | Article 4

https://doi.org/10.15447/sfews.2026v24iss3art4

* Corresponding author: sgonsalves@anchorqea.com

1 Anchor QEA, Inc.
Portland, OR 97219 USA

2 Columbia Basin Research
School of Aquatic and Fishery Sciences
University of Washington
Seattle, WA 98101 USA

3 Flow West
Oakland, CA 94604 USA

INTRODUCTION

The Sacramento–San Joaquin Delta (Delta) is the tidally influenced freshwater portion of the San Francisco Bay estuary, which flows into the Pacific Ocean. San Joaquin River (SJR) tributaries represent the southernmost distribution of Chinook Salmon (*Oncorhynchus tshawytscha*) in California's Central Valley (CV), although the current southernmost component of the fall-run Chinook Salmon population on the Merced River is heavily supported by hatchery production (Yoshiyama et al. 2000). While fall-run Chinook Salmon are the most abundant of the CV runs and support the ocean fishery off the coast of California, most of these fish are of Sacramento River-origin (PFMC 2023), and a large portion are hatchery produced (Williams 2006). Adult fall-run escapement in the SJR system has been highly variable since at least the 1950s (Williams 2006), with in-river spawner numbers in all tributaries ranging from greater than 70,000 in some years to below 1,000 during the 1990s and generally declining over time to the present (Azat and Killam 2024, as available on CBR 2024).

The CV fall/late-fall-run Chinook Salmon Distinct Population Segment (DPS) is not currently listed under the Endangered Species Act but is considered a species of concern (Crozier et al. 2019). Physical habitat changes, altered flows, water diversions, nutrient and contaminant inputs, climate extremes, and nonnative plants and fish species have resulted in increasingly challenging conditions in SJR and Delta ecosystems since the late 1800s (Nichols et al. 1986; McEwan 2001; Luoma et al. 2015). Primary threats for the CV fall/late-fall-run Chinook Salmon DPS currently include genetic homogenization from high hatchery production, the warming marine climate, the highly altered freshwater habitat in the Delta, and the DPS's specialized life-history strategies (Williamson and May 2005; Crozier et al. 2019). The cyclical variation in SJR adult abundance has been hypothesized to relate to river flow during the spring juvenile out-migration period (SJRGA 2013; Towne et al. 2022). Higher flows are expected to increase juvenile salmonid survival by improving water quality and reducing travel time (Newman 2003; Kimmerer 2008; Lehman et al. 2017; Towne et al. 2022). However, point estimates of juvenile fall-run through-Delta survival have been consistently near or below 10% since the early 2000s, despite this period encompassing several hydrologically "wet" water years (Buchanan, Barnard, and Brandes 2018).

The Delta encompasses a complex network of natural channels and canals that branch off or join the mainstem river, creating multiple migration routes for juvenile fish. The primary alternative to the mainstem migration route for SJR-origin fish is the Old River route. Old River is the first major distributary junction that fish encounter, and leads to the interior South Delta, where the State Water Project (SWP) and federal Central Valley Project (CVP) combined can export up to 436 cubic meters per second (m^3 s^{-1}) of water to municipal and agricultural water users throughout California (ESA and AECOM 2018). SWP and CVP operations can affect the hydrodynamics throughout much of the interior South Delta (SST 2017b). High mortality for juvenile salmonids in the interior Delta is thought to relate to hydrodynamic patterns that confuse or entrain juvenile salmonids near the water projects (SST 2017a), high predation (Vogel 2011; Grossman 2016), and reduced water quality—conditions that may be intensified by water project operations in conjunction with other ongoing urban and agricultural water and land-use practices (NMFS 2009). However, in some years, over 65% of tagged juvenile Chinook Salmon that survive to exit the Delta at Chipps Island do so by being entrained at the CVP Tracy Fish Collection Facility and transported downstream by truck (Buchanan, Barnard, and Brandes 2018).

Environmental and hydrodynamic conditions are hypothesized to be linked to juvenile salmon survival outcomes through behavioral responses (SST 2017a), including swimming behavior and diel activity patterns that juvenile salmon may use to rest, search for food, or avoid predators, (Lehman et al. 2017; Nobriga et al. 2021). A study of juvenile Chinook Salmon swimming behavior at the head of Old River junction showed that fish exhibited swimming with and against the

direction of current, passive transport, and lateral (i.e., cross-channel) swimming (Holleman et al. 2022). At a coarser scale, juvenile steelhead movements between hydrophone arrays near the pumping facilities were not clearly directed downstream but instead were strongly influenced by twice-daily tidal cycles, upstream-directed net channel flow caused by South Delta water project operations and release day (Anchor QEA 2022). A similar study of juvenile Chinook Salmon movements at distributary junctions with the mainstem SJR found that downstream movements increased with ebb tides and downstream-directed net flow and decreased with flood tides (Dodrill et al. 2022). Localized hydrodynamic conditions were found to account for more variation in steelhead movements out of river junctions on the SJR mainstem than remote conditions or daily average flow and export rates (Buchanan 2024).

In this study, we used 8 years of an existing dataset of acoustic telemetry detections of juvenile SJR-origin fall-run Chinook Salmon in the Delta to relate salmon movements to environmental conditions and operational actions in the interior South Delta near the water projects. The dataset used was previously collected as part of the Vernalis Adaptive Management Plan (VAMP) Salmon Smolt Survival Investigations (2010 to 2011) and the South Delta Chinook Salmon Survival Studies (2012 to 2017). These data have been used previously by other researchers to evaluate juvenile Chinook Salmon survival and route choice through the Delta (Buchanan et al. 2013; Buchanan, Barnard, and Brandes 2018; Buchanan and Skalski 2020) and movements at mainstem junctions (Dodrill et al. 2022). We related juvenile salmon movements to simulated outputs from a well-validated, high-resolution, 3-D hydrodynamic model developed for the San Francisco Bay and Delta (MacWilliams et al. 2015) using a continuous-time multi-state Markov model (Jackson 2011). Use of a hydrodynamic model allows data to be extracted at the fish detection locations (i.e., at telemetry arrays) without needing to extrapolate over locations or time-periods of missing data that commonly occur in river-gage data, while the multi-state framework facilitates analysis of individual fish movement histories through various physical locations ("states"). Assuming that juvenile salmonids use flow as a migration cue, we hypothesized that movements would be influenced primarily by the direction of net channel flow, but that fish would also "go with the flow" by making movements that coincide with local flow variations resulting from tidal influence or water project operations. Entrainment of juvenile Chinook Salmon into a large forebay was expected to be related to gate opening and closing operations at the forebay entrance, and we hypothesized that there would be a diel pattern of movements related to predator avoidance in this high-predation area.

MATERIALS AND METHODS

Study Area

The Delta is formed at the confluence of the south-flowing Sacramento River, the north-flowing SJR, and other tributaries, including the Mokelumne and Cosumnes rivers. Historically, the Delta consisted of approximately 3,000 square kilometers (km^2) of tule marsh and low-lying forested islands that connected meandering channels from California's CV to the Suisun, San Pablo, and San Francisco bays and on to the Pacific Ocean (Luoma et al. 2015). Delta habitat is now highly modified, with most channels leveed, and land use converted to a mix of agriculture and urban development (Luoma et al. 2015).

Our study area, which we term the water project area (WPA; Figure 1), is a convergence of multiple waterways in the southwestern Delta including in the southwestern Delta including Old River, Grant Line and Fabian Bell Canal, West Canal, and Victoria Canal, with inlets to Jones Pumping Plant (part of the CVP; owned by the US Bureau of Reclamation (Reclamation) and, through the Clifton Court Forebay radial gates, to Harvey O. Banks Delta Pumping Plant (part of the SWP; owned by the California Department of Water Resources [CDWR]). West Canal conveys flow from Old River and Grant Line and Fabian Bell Canal past the Clifton Court Forebay radial gates before reconnecting with Old River. Flow in West Canal is often reversed (i.e., flowing upstream

https://doi.org/10.15447/sfews.2026v24iss3art4

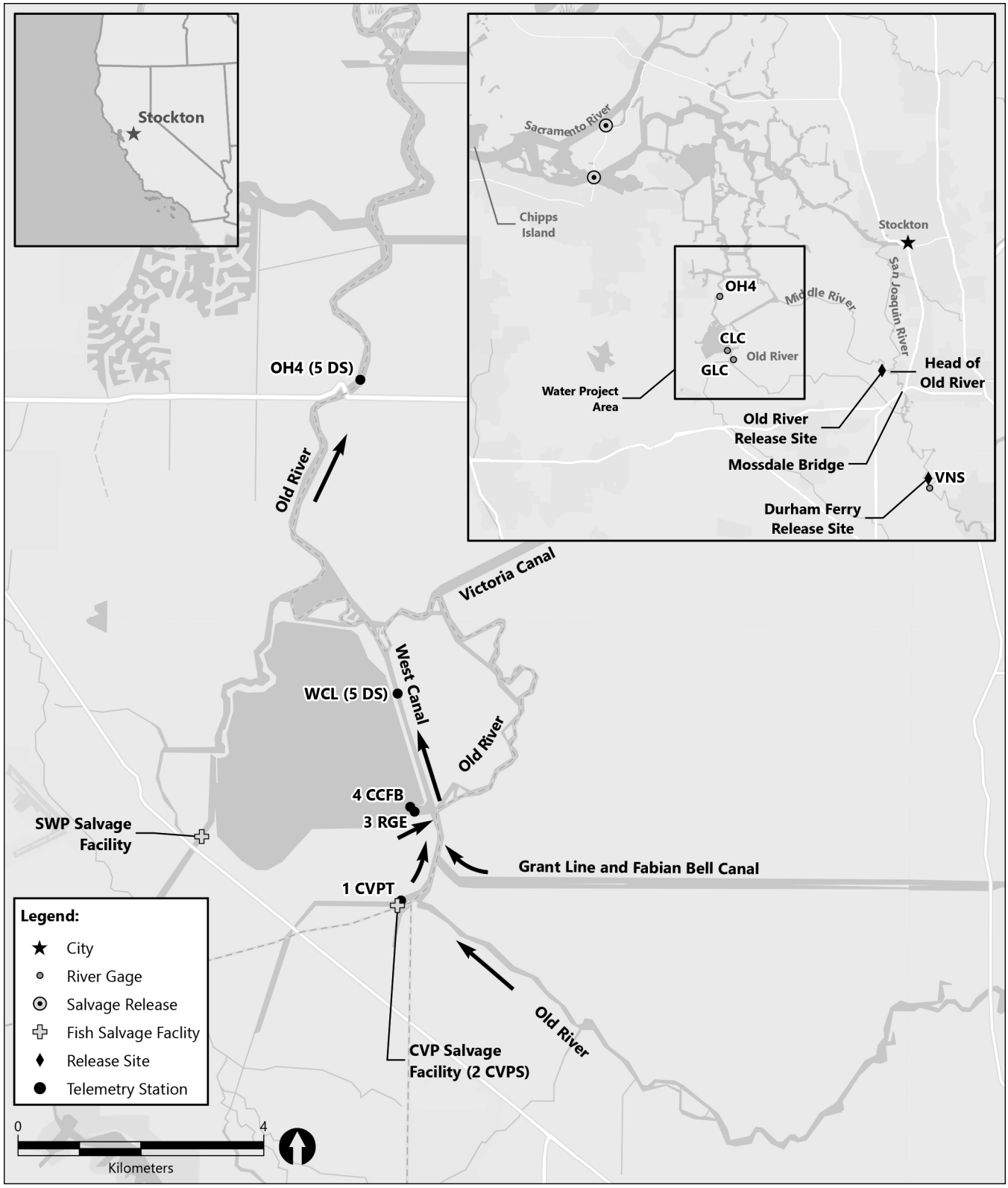

Figure 1 Water project area (WPA) vicinity. *Black arrows* show the direction of positive flow in the UnTRIM model. Numbered locations refer to states in the multi-state model. Inset maps show the South Delta (*top right*) and state of California (*top left*).

[south]) depending on SJR Delta inflow, export demands, and operational requirements. SJR Delta inflow is measured at the river gage station (station ID: VNS; CDWR c2024) located just east of Vernalis, California, near the Durham Ferry Road bridge (Durham Ferry).

Outmigrating Chinook Salmon enter the South Delta at Mossdale Bridge near Lathrop, California, approximately 16 kilometers (km) downstream of Durham Ferry. In the Delta, juvenile salmon must travel approximately 90 km on the SJR mainstem route or through the interior South Delta to Chipps Island at the entry to Suisun Bay. During this journey, juvenile fish encounter natural river junctions, sloughs, and side channels as well as human-made canals, diversions, and infrastructure (e.g., forebays and gates). Conditions at these junctions determine fish behavior and routing through the Delta, and may influence overall survival, depending on spatial heterogeneity in survival among migration routes (Perry et al. 2010, 2013; Buchanan, Barnard, and Brandes 2018). The first junction fish encounter after entering the South Delta is the bifurcation of the SJR and Old River (i.e., the head of Old River, HOR), approximately 4.6 km downstream (north) of Mossdale Bridge. Routing at this junction is important because it determines whether fish will turn westward into the interior South Delta and toward the WPA.

A major factor that determines whether fish will enter Old River is installation of a temporary barrier at HOR. From 1992 until 2018 (CDWR c2023), a temporary physical (rock) or non-physical barrier (bubble curtain) was installed at HOR in the springtime in many years, although it was not installed when SJR inflow exceeded 141.6 $m^3 s^{-1}$, and it is no longer installed as a result of changes in regulatory requirements (CDWR c2023). The barrier was installed under the assumption that diverting fish and flow into the mainstem SJR would increase their survival. In years when the barrier was not installed, 42% to 77% of acoustic-tagged hatchery Chinook Salmon released upstream on the SJR were observed taking the Old River route toward the WPA (Buchanan et al. 2013).

Routing in the WPA is thought to be strongly driven by both export pumping and tidal influences (SST 2017a). Juvenile Chinook Salmon that travel northward on West Canal and continue north along Old River can leave the Delta by re-entering the northern (downstream) end of the SJR and completing their migration toward Chipps Island. Juvenile salmon may also be entrained and salvaged at the Tracy Fish Collection Facility or the Skinner Fish Facility, parts of the CVP and SWP water export facilities, respectively (Buchanan, Barnard, and Brandes 2018). Salvaged juvenile salmon are trucked overland to a release location approximately 20 km upstream of Chipps Island (Buchanan et al. 2021).

Telemetry Data

An existing 8-year (2010 to 2017) acoustic telemetry dataset of South Delta juvenile fall-run Chinook Salmon was retrieved from the National Oceanic and Atmospheric Administration's Environmental Research Divisions Data Access Program (NOAA-2025a and 2025b) and used for this study. Fish tagging and telemetry field methods are described briefly in Appendix A, and in detail in a series of annual reports (SJRGA 2011, 2013; Buchanan et al. 2015, 2016; Buchanan, Brandes, and Ingram 2018;

Buchanan, Brandes, and Skalski 2018; Barnard et al. 2022; Towne et al. 2022). The fish used in this study were released either on the SJR near Durham Ferry or in Old River just downstream of HOR (Table 1), and had fork lengths that ranged from 73 to 140 millimeters (mm) (Buchanan, Barnard, and Brandes 2018; Barnard et al. 2022; Buchanan and Whitlock 2022b).

Acoustic telemetry data were collected on stationary hydrophone and receiver arrays deployed throughout the Delta. For this study, we selected a subset of the original telemetry dataset that included only the detections from acoustic receivers located in the WPA. Detections were used from the CVP Tracy Fish Collection Facility (CVP salvage [CVPS]) and from arrays co-located with simulated hydrodynamic data outputs: CVPT (CVP trash racks), RGE (just outside the Clifton Court Forebay radial gates), CCFB (inside the

https://doi.org/10.15447/sfews.2026v24iss3art4

Table 1 Summary of acoustic-tagged fish release numbers (N_{Rel}), locations, and dates; WPA fish-detection numbers (N_{Study}) and dates; SJR Delta hydrologic conditions; and head of Old River (HOR) barrier conditions

Year	Release dates	NRel	Release location	Release water temperature (˚C)	WPA detection dates	NStudy	Water year type[a]	Spring SJR Delta inflow[b] (m^3s^{-1})	HOR barrier type
2010	27 April–19 May	504	Durham Ferry	15.6–18.8	28 April–2 June	135	Above normal	124 ± 28	Bubble/ sound
	28 April–20 May	247	Old River	14.2–17.5	28 April–29 May	151			
2011	17 May–19 June	1,895	Durham Ferry	14.0–18.8	18 May–4 July	370	Wet	463 ± 199	None
2012	2–22 May	959		17.5–20.7	5 May–1 June	4	Dry	65 ± 23	Rock
2013	1–19 May	950		16.8–20.3	3 May–2 June	81	Critical	50 ± 34	None
2014	16 April–19 May	1,918		15.9–22.1	20 April–30 June	6	Critical	34 ± 27	Rock
2015	15–30 April	799		15.4–24.7	—	0	Critical	14 ± 9	Rock
2016	13–22 April	648		17.6–20.4	17 April–7 May	6	Dry	40 ± 25	Rock
2017	12–28 April	647		13.7–15.1	14 April–15 May	86	Wet	541 ± 125	None

a. Water year type is a hydrologic classification for the San Joaquin Valley based on SJR unimpaired runoff, and is assigned by CDWR (c2025a).
b. The mean SJR Delta inflow at Vernalis, California (VNS gage), is given for April through June for each year, with standard deviation (CDWR c2025a).

Clifton Court Forebay near the radial gates), WCL (West Canal), and OH4 (Old River at Highway 4) (Figure 1). At each array location, multiple hydrophones were deployed in one or more cross-channel lines to ensure stream channel coverage and increase detection probability, except for CVPS, where receivers were deployed directly into salvage tanks. Based on a concurrent study of juvenile steelhead through the Delta, acoustic detection probabilities were generally greater than 90% during the telemetry study, though in some years individual arrays and release groups had low detection probability or detection probability could not be calculated (Buchanan et al. 2021).

Raw acoustic receiver detection data were processed into detection events for each tag by US Geological Survey laboratories in Cook, Washington (2010, 2011) and Sacramento, California (2012 to 2016) and at the Great Lakes Science Center (2017). A detection event was defined as a series of detections of a single fish tag on a single acoustic receiver at an array location with 30 minutes or less between individual detections, uninterrupted by detection elsewhere. For this study, detection events were further combined to include all concurrent or overlapping detection events by multiple receivers at an array location. Fish were considered to be continuously present at a location during a detection event. Fish were required to have at least two detection events in the WPA to be included for analysis.

A predator filter based on observed behavioral differences between juvenile Chinook Salmon and resident predatory fish—such as juvenile and sub-adult bass—was applied to the telemetry data (Buchanan and Whitlock 2022a; see additional description in Appendix A). All detection events that triggered the predator diagnosis were removed from the dataset, along with all subsequent detections of the predated tag. However, uncertainty about the timing and location of the actual predation event meant that some predated detections may have remained in the filtered dataset. To avoid biasing the analysis of fish movement with detections that may have occurred after a predation event, fish detection histories with very long residence times (up to 50 days) at a single location and that triggered the predator filter upon leaving a location were censored at 12 days, following a preliminary analysis (see additional description in Appendix A).

Fish Movement Modeling

Fish transitions—defined as movement between telemetry stations in the WPA—were modeled using a continuous-time multi-state Markov model (Jackson 2011) in which individuals move from

state *r(t)* at time *t* to state *s(t + dt)* at time *t + dt*. In the model, the fish's state at time *t* depends only on its state at time *t−1*. Models were fit using the 'msm' package (version 1.7.1; Jackson 2011, 2023) in R version 4.4.2 (R Core Team 2021), which assumes parametric distributions for transition rates and transition times, and estimates parameters using the principle of maximum likelihood. Transitions between states were characterized by a transition rate matrix *Q(t)* whose elements *qrs(t)* represented the instantaneous risk of transitioning from state *r* to state *s* (Figure 2). The diagonal elements of the transition rate matrix, q_{rr}, represented the risk of remaining in the same state (*r*) from one 30-minute time-step to the next, and were defined to be equal and opposite of the total risk of moving to another state, $q_{rr} = -\Sigma_{s \neq r} q_{rs}$; thus, each row of the matrix summed to zero. The time lapse between state transitions was assumed to be an exponentially distributed random variable, with rate $\lambda = -q_{rr}$ and with a mean time to transition of $1/\lambda = -1/q_{rr}$. Data used in the analysis consisted of a time- series of occupied states for each fish, *S(t = 0), S(t = 1), ..., S(t = n)* for *t* = 0, 1, ..., *n* time-steps after first entering the WPA.

Upon entering the WPA, each tagged fish was assigned to one of four transient states and one absorbing state (i.e., a state from which fish cannot transition away) that represented locations in the WPA. Transient model states were 1 CVPT, 3 RGE, 4 CCFB, and a downstream state 5 DS (Figure 2). The downstream (DS) state combined detections at the WCL telemetry array and the OH4 array because the WCL array was not deployed every year. One state, 2 CVPS, was considered an absorbing state, and fish were allowed to enter CVPS only from CVPT. For example, if a fish was observed at RGE and then next observed at CVPS, the model assumed that the fish passed through CVPT. The transition rate matrix for the fish movement model had the following form for a given time-step:

$$Q = \begin{bmatrix} q_{11} & q_{12} & q_{13} & q_{14} & q_{15} \\ q_{21} & q_{22} & q_{23} & q_{24} & q_{25} \\ q_{31} & q_{32} & q_{33} & q_{34} & q_{35} \\ q_{41} & q_{42} & q_{43} & q_{44} & q_{45} \\ q_{51} & q_{52} & q_{53} & q_{54} & q_{55} \end{bmatrix} = \quad \text{Eq 1}$$

$$\begin{bmatrix} -(q_{11}+q_{13}+q_{15}) & q_{12} & q_{13} & 0 & q_{15} \\ 0 & 0 & 0 & 0 & 0 \\ q_{31} & 0 & -(q_{33}+q_{34}+q_{35}) & q_{34} & q_{35} \\ 0 & 0 & q_{43} & -q_{43} & 0 \\ q_{51} & 0 & q_{53} & 0 & -(q_{51}+q_{53}) \end{bmatrix}$$

Exact fish arrival and departure times from a state were retained regardless of the time-step at which model covariates changed. An observation type that indicated a known transition time was used for detections on consecutive time-steps at the same state (i.e., during a single detection event) because the fish was assumed to be continuously present in that state. The model also included indeterminate observations for all time-steps when the covariates changed but the fish was not detected, as well as for fish detections after a gap of >30 minutes. An indeterminate observation indicates that the state the fish was in since the prior time-step was unknown, and the current state *s(t)* of the fish was allowed to be either known or unknown (i.e., censored state) (Jackson 2023). A censored state indicates that the true state could have been any of the transient states in the model. An example fish detection history is provided in Figure A-1 of Appendix A.

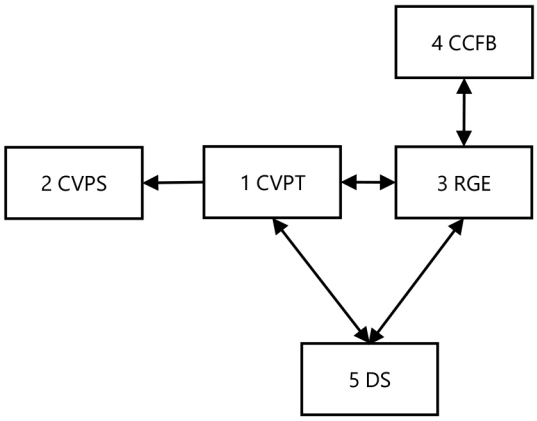

Figure 2 Multi-state fish movement model diagram. Model states correspond to the following telemetry detection locations, shown in Figure 1: CVP trash racks (1 CVPT),CVP salvage (2 CVPS), just outside Clifton Court Forebay radial gates (3 RGE), inside Clifton Court Forebay near the radial gates (4 CCFB). West Canal (WCL) and Old River at Highway 4 (OH4) detection locations are combined into 5 DS.

https://doi.org/10.15447/sfews.2026v24iss3art4

We expressed the transition rates in matrix Q as functions of covariates using a proportional hazard model as follows:

$$q_{rs}(z_i(t)) = q_{rs}^0 \exp(\beta_{rs}^T z_i(t)) \quad \text{Eq 2}$$

where $z_i(t)$ is a vector of covariates for individual i at time t, q_{rs}^0 is the baseline transition rate, β_{rs} is a vector of regression coefficients for the covariates $z(t)$, and $\exp(\beta_{rs})$ is a vector of hazard ratios. Transition rates (q_{rs}) express how likely it is that a fish will make a given transition; hazard ratios ($\exp(\beta_{rs})$) represent the relative effect of a covariate on the transition rate compared to the baseline rate (Jackson 2023).

The estimated transition probability matrix from a fitted continuous-time multi-state model can be calculated for a given time interval at a given set of covariate values by assuming a time-homogenous process (Jackson 2023). Conditional on a transition not having occurred by time t, the probability of transitioning from state r to state s from time t to time $t + u$ was calculated as the following:

$$P(t+u|z(t)) = exp\{uQ(z(t))\} \quad \text{Eq 3}$$

where $P(t + u|z(t))$ is a u-time-step transition probability matrix conditional on covariates $z(t)$, $Q(z(t))$ is the transition rate matrix, which is constant over time t to time $t + u$ and depends on covariates $z(t)$, and "exp" is the matrix exponential. The elements of the transition probability matrix $P(t + u)$ are $p_{rs}(t + u)$, the probability of transitioning from states r to s in u time-steps, given the covariate values during time-step t. To isolate the effect of individual variables, we estimated time-homogenous transition probabilities over the variable range that occurred in the data and over a period of time (1 hour, $u = 2$) for which the time-changing variable could reasonably be approximated by a constant value.

To account for a non-homogeneous process, where Q varies with time-dependent covariates but can be approximated as a piecewise constant, we calculated the transition probability matrix as a product of matrices over a series of intervals (Jackson 2023). The probability matrix that represents state transitions over a longer time-period, during which the covariate values changed, is defined as $P(t, u)$, for $u > t$, which is calculated in a piecewise manner as follows:

$$P(t,u) = P(t+1|z(t))P(t+2|z(t+1)) \cdots P(u|z(u-1 \quad \text{Eq 4}$$

Covariates

We hypothesized that hydrodynamic (flow and operations), environmental, and fish-related variables would affect transition rates, and we used these variables in modeling fish movements (Table 2).

Flow and Operations from Hydrodynamic Modeling. For this study, we simulated hydrodynamic variables using the UnTRIM Bay–Delta model (UnTRIM model). The UnTRIM model is a high-resolution 3-D hydrodynamic model of the Bay–Delta that extends from the Pacific Ocean through the entire Delta. Model development is described by MacWilliams and Cheng (2007), MacWilliams and Gross (2007, 2013), and MacWilliams et al. (2008, 2009, 2015), and has previously been used in fish analyses (MacWilliams et al. 2016; Anchor QEA 2022; Buchanan 2024). A high-level overview of UnTRIM model history, methods, model validation, and use in other Bay–Delta studies can be found in Anchor QEA (2022).

Simulated data from the UnTRIM model represent predictions of the physical conditions a fish would have experienced at the time of detection and were extracted for time- periods that overlapped with the telemetry data during each year (Table 1). Cross-sectional water flow, depth-averaged water temperature, and percent source water (Table 2) were extracted directly from the model at each location that corresponded to the states included in the fish movement model (except for CVPS). Conditions at OH4 were generally highly correlated with conditions at WCL; therefore, we selected hydrodynamic outputs at WCL to model the DS state. We discarded some variables

Table 2 Covariates evaluated in fish-movement modeling

Name	Type[a]	Units	Description	Time-step[b]
Flow.net	Flow and operations	$m^3 s^{-1}$	Net discharge flow at the fish detection location (CVPT, RGE, WCL). Calculated by smoothing total discharge with a double rolling mean over the length of the daily tidal cycle (24.8 hours)	90-second
Flow.tdl	Flow and operations	$m^3 s^{-1}$	The tidal component of flow at CVPT or WCL. Calculated by subtracting the net discharge flow from the total discharge at these locations. Not calculated at RGE because of the step-like pattern caused by radial gate opening and closing (see Flow.RGE).	90-second
Flow.RGE	Flow and operations	$m^3 s^{-1}$	Total flow at RGE. Constructed using open and closure gate operations information. When the gates are open, flow is generally constant; when gates are closed, flow is approximately 0, as shown in Figure 3.	90-second
Temp.mean Temp.max Temp.cont	Environmental	°C	Daily mean, daily maximum, and continuous water temperature at the fish-detection location.	Daily Daily 3-minute
Turb	Environmental	NTU/FNU[c]	Turbidity at the nearest stream gage to the fish-detection location.	15-minute
Chl	Environmental	$\mu g L^{-1}$	Chlorophyll concentration at the nearest stream gage to the fish- detection location.	15-minute
SJRW.pct	Environmental	%	The percent SJR water at the fish- detection location.	3-minute
Fish.length	Fish size	mm	Fish fork length at tagging	Constant
RG.ind	Operations indicator	Unitless	An indicator for the radial gates being open (1) or closed (0).	90-second
Night.ind	Fish indicator	Unitless	An indicator for nighttime (1) or daytime (0). Nighttime is defined as being from sunset to sunrise at a central latitude and longitude in the Delta.	Bi-daily
OR.ind	Indicator	Unitless	An indicator for release at Old River (1) or Durham Ferry (0).	Constant
LRCen.ind	Indicator	Unitless	An indicator for fish that triggered the predator filter for long residence time and therefore have a right-censored detection history (1) or all other fish (0)	Constant

a. Environmental and flow variables were measured (Turb, Chl) at river gage locations, or simulated (Flow and Temp variables) using the UnTRIM model at receiver locations that represented states in the multi-state model.
b. Original time-step of variables as exported from the UnTRIM or collected at river gages operated by the US Geological Survey and CDWR. Before inclusion in the multi-state models, continuous variable time-steps were reduced to the 30-minute time-step of the fish-movement model.
c. Nephelometric turbidity unit/formazin nephelometric unit.

available from the UnTRIM model either for being nearly constant during the periods that fish were present (depth-average salinity) or for being highly correlated with the retained variables (depthaveraged current velocity and water depth were both highly correlated with cross-sectional water flow). In the UnTRIM model, the assumed direction of positive flow in the WPA is away from the CVPT and radial gates and in the downstream (i.e., northward) direction in West Canal and Old River (Figure 1). In the extracted variables, the direction of water flow was indicated by the sign of the flow metric.

In the Delta, percent source water can vary both with natural inputs and with water project exports, which pulls water from the Sacramento River and tributaries— such as the Mokelumne River—into the South Delta. Percent source water may affect the ability of fish to cue to natal stream water to navigate on their outward migration. To disentangle the influence of riverine flow from tidal variations, we computed net river flow as the double moving average of total flow over the daily tidal-cycle period (approximately 24.8 hours) at locations included in the model (Figure 3). We calculated the tidal component of flow as total flow minus net flow at the same locations. The step-like flow pattern of total flow at RGE reflected the opening and closing of the gates for operations (Figure 3C). We included an indicator variable that defined when the radial gates were open to evaluate the effect of opening and closing operations, apart from flow. Flow conditions in the WPA reflect water project exports as well as Delta inflow and tides. We interpreted the net flow measures at CVPT and RGE to represent "export flow" at these locations because negative net flow at CVPT represents flow into the Delta Mendota Canal of the CVP, and negative net flow at RGE represents flow into Clifton Court Forebay of the SWP. Because the

https://doi.org/10.15447/sfews.2026v24iss3art4

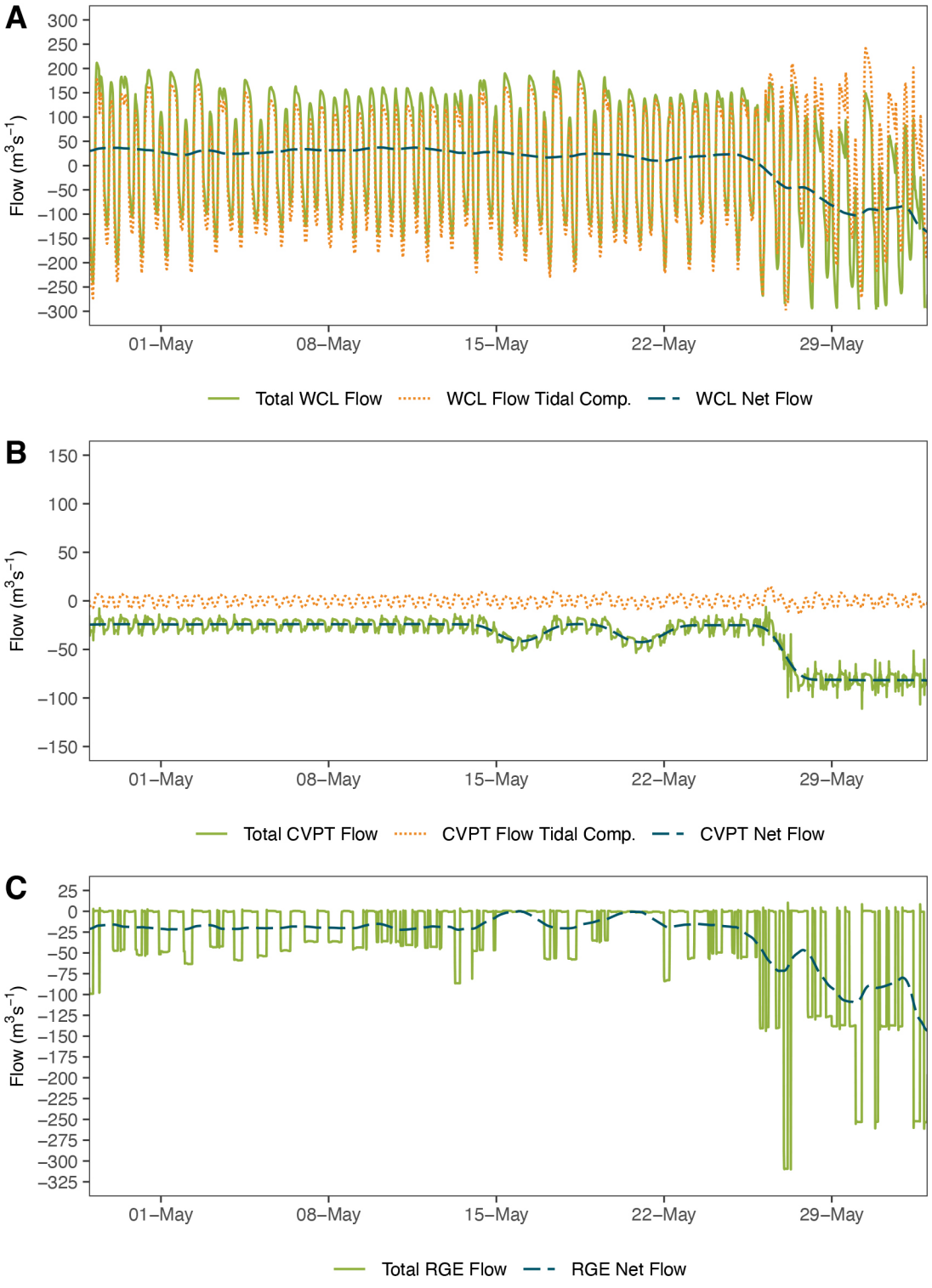

Figure 3 Simulated flow outputs from the UnTRIM model during fish presence in the water project area (WPA) in 2010 at (**A**) WCL, (**B**) CVPT, and (**C**) RGE

assumed direction of positive flow is downstream, "export flow" is represented by negative net flow at CVPT and RGE.

Environmental Conditions. Environmental variables included in the fish movement model were water temperature metrics, turbidity, and chlorophyll (Table 2). We selected these environmental variables because higher water temperatures and turbidity can reduce the swimming performance of Chinook Salmon (Lehman et al. 2017), and high levels of chlorophyll also indicate poor water quality that could affect the condition and movements of fish.

We retrieved turbidity and chlorophyll data from river gages at locations in or near the WPA and where continuous or nearly continuous data were available for the same years as the juvenile Chinook Salmon telemetry dataset (Table 1; CDWR c2024). We retrieved data from the Grant Line Canal gage (station ID: GLC), Clifton Court Forebay gage (station ID: CLC), and Old River at Highway 4 gage (station ID: OH4). We interpolated missing data using daily, weekly, or (in one case) monthly median values. We used data from the CLC gage to model transitions into and out of the CCFB, from the GLC gage for transitions away from CVPT and between RGE and CVPT, and from the OH4 gage for transitions away from DS and RGE to DS.

Fish Variables. The fish-related variables considered for analysis were fork length, release day, and an indicator of nighttime (Table 2). We discarded release day during data exploration because it was highly correlated with net flow in West Canal, water temperature, and fork length. We included fork lengths because they varied by study year (see Appendix A). We included a nighttime indicator because studies of migrating salmonid smolts have identified nocturnal migration behavior (Chapman et al. 2013) and increases in activity during the day (Smith et al. 2021), although some studies reported no detected effects (Buchanan et al. 2021). An analysis of juvenile steelhead at the HOR found an increase in movements at night when the rock barrier was installed (Anchor QEA 2022). We assigned nighttime based on central Delta latitude and longitude coordinates and using the R package 'suncalc' (Thieurmel and Elmarhraoui 2022). We included two additional indicators as nuisance variables to account for the effects of downstream release at Old River (in 2010 only) and the censoring of long residence time in the detection histories.

Covariate Models

To develop alternative models for covariates, we first built a baseline model that included the available indicators. Next, we fit single-variable covariate models to determine candidate covariates for each transition. We developed multi-variable models by considering additional covariates for each transition based on performance in single-variable modeling.

All models included the indicators for time of day, Old River release, and long residence censoring. Therefore, the baseline model had the following form:

$$q_{rs} = q_{rs}^{0} exp(\beta_1 OR.ind + \beta_2 LRcems.ind + \beta_3 Night.ind) \quad \textbf{Eq 5}$$

We dropped indicator variables from specific transitions in the model before we added additional covariates if the 95% confidence interval (CI) of their associated hazard ratio (HR) had width >2 orders of magnitude and included the value 1 (equivalently, if the 95% CI for the estimated regression coefficient included 0). Very wide CIs that include 1 for HRs suggest that there is no information in the data about the corresponding effect (Jackson 2023) and complicate interpretation of the effects of other covariates. We used this same decision process for determining variable "importance" from the HR 95% CI in subsequent steps of modeling to decide whether to retain or remove variables. Before inclusion in modeling, we standardized all continuous covariates to have a mean of zero and unit standard deviation and processed each to a 30-minute time-step.

We developed single-variable transition models to explore operational and environmental effects on each possible movement. Because of limited

https://doi.org/10.15447/sfews.2026v24iss3art4

sample size (n = 8), we did not model covariate effects for the 5 DS→1 CVPT transition. In general, we matched explanatory variables to the location closest (closest river gage, or extracted at the exact location from the UnTRIM model) to the transition starting location. For example, we used temperature at CVPT to model the transition from 1 CVPT→3 RGE, whereas we used temperature at RGE for the reverse transition from 3 RGE →1 CVPT. For flow, however, we considered that all transitions might be driven by a single operational aspect in the WPA, such as the opening and closing of the radial gates and the associated flow; therefore, we developed models that applied flow from a single site (e.g., net flow at CVPT) to all transitions. We then developed a "Local Flow" model that used the closest or most influential local flow variable for each transition; for example, flow at CVPT (Flow.CVPT.net or Flow.CVPT.tdl) for transitions away from CVPT (1→2, 1→3, and 1→5), or flow in West Canal (Flow.WCL.net or Flow.WCL.tdl) for transitions when fish had to traverse the West Canal/Old River channel (e.g., from DS to RGE [5→3]).

We compared single-variable models using likelihood-based inference. We used a likelihood ratio (LR) test to determine whether single covariate models were better than the baseline indicator model and used Bonferroni corrections to account for multiple testing (Sokal and Rohlf 1995). We used the single-variable model with the highest LR and important HR effects on multiple transitions was used as the basis of the next step in developing a multi-variable model.

We built candidate multi-variable models in a three-step sequence based on variable performance in single-variable modeling:

1. We started with the best performing single-variable flow model and added the best performing environmental variable.

2. We added the complementary component of flow for each transition (e.g., if net flow was applied to a transition, we added tidal flow); for the radial gates, we added the opening–closing indicator.

3. We then simplified the model by dropping covariates from specific transitions where the covariate effect was unimportant.

We used the small sample-size corrected Akaike Information Criterion (AICc; Hurvich and Tsai 1989; Burnham and Anderson 2002) to evaluate the three candidate multi-variable models while accounting for the large number of estimated parameters (k = 29–53) compared with the sample size (n = 745 observed transition events). We evaluated collinearity by confirming that the variance inflation factor among covariates was < 3. We evaluated model goodness-of-fit by visually comparing the observed vs. fitted prevalence (i.e., numbers) of fish in each state over time (Jackson 2023) and examining model residuals for the presence of individual fish with outlier detection histories (see the description of the model's evaluation in Appendix B).

We examined the effects of covariates on transition rates as follows: (1) use the sign and magnitude of the HRs or slope coefficients to represent their effect on transition rates; (2) plot the effect of each covariate on the 1-hour (u = 2) probability of transition when the remaining covariates were held at their mean or median values using Equation (3); and (3) plot piecewise transition probabilities over a 3day period during which study fish were present and covariates such as flow changed at each time-step. Piecewise transition probabilities reflect the effects of changing conditions and time of day on fish movements over the 3-day period for hypothetical juvenile Chinook Salmon that entered the WPA at the start of the first day. We used the fitted multi-variable model from Equation (4) to predict transition probabilities over two 3-day periods when fish were present and that represented a wide range of flow and operational conditions: (1) from 18–20 June 2011, a wet water year (WY) period when 81 to 87 fish were detected daily in the WPA; and (2) from 20–22 May 2013, a critical WY period when 35 to 40 fish were detected daily in the WPA.

RESULTS

Environmental Conditions

Conditions in the SJR watershed were hydrologically above normal and wet in WYs 2010 and 2011, respectively, followed by 4 years of dry to critically dry conditions in WYs 2012 to 2016, and wet conditions in WY 2017 (CDWR c2025b). Springtime juvenile Chinook Salmon release dates varied by year, occurring as early as April 12 in 2017 and as late as June 19 in 2011, and fish generally arrived downstream in the WPA between April and June, though in 2011 fish were present in the WPA until July 4 (Table 1). The mean daily SJR Delta inflow at Vernalis in April through June ranged from 124 $m^3 s^{-1}$ in 2010 to 541 $m^3 s^{-1}$ in 2017 in the above-normal and wet water years, and from 14 $m^3 s^{-1}$ in 2015 to 65 $m^3 s^{-1}$ in 2012 in the drought years (Table 1; CDWR c2025a). During the periods when fish were present in the WPA, median net flow in West Canal was reversed (i.e., negative) in all years, except 2010 and 2017 (Figure 4).

In the WPA, fish experienced median daily mean water temperature (DMWT) of approximately 20 °C (range: 19.9 °C to 20.5 °C) during the drought years (2012 to 2014), except in 2016 when median DMWT was slightly cooler (approximately 18.5 °C). In the wetter years of 2010 and 2017, median DMWT was 3.2 °C to 4.5 °C cooler (range: 15.9 °C to 16.7 °C) (Figure 4). Although 2011 was the second-wettest water year, later fish releases in June resulted in juvenile Chinook Salmon being exposed to a warmer median DMWT (range: 18.5 °C to 19.1 °C) in the WPA from late June to early July. A study-wide maximum DMWT of 24.1 °C occurred at WCL in 2011. Median percent SJR water in the WPA was above 85% (range: 51.3% to 99.8%) in the above-normal and wet water years and below 60% (range: 1.0% to 96.8%) in the dry and critical water years (Figure 4). Turbidity in the WPA was generally low; median turbidity at all three river gage locations was < 23.5 nephelometric turbidity units (NTU) in all years, though turbidity events above 100 NTU

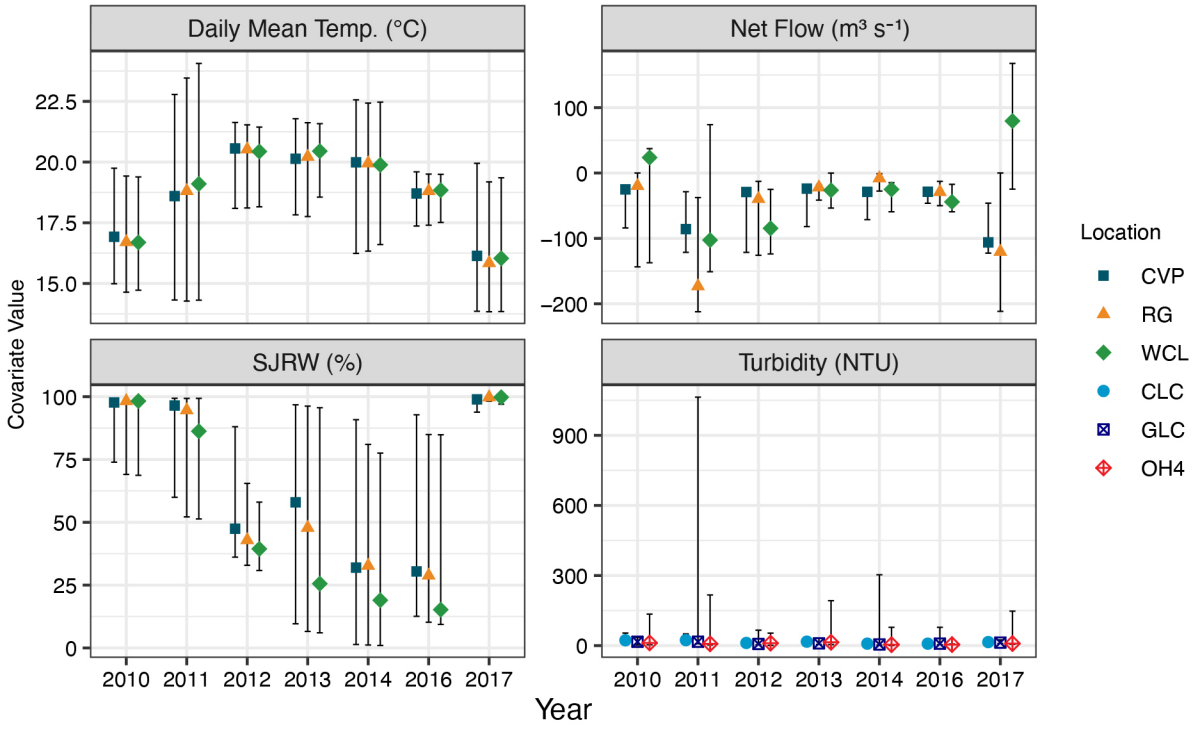

Figure 4 Environmental conditions during fish presence in the water project area (WPA). Panels show the median (*points*) and range (*black lines*) for each parameter. Water temperature, net flow, and San Joaquin River water percent (SJRW) were exported from the UnTRIM model at the locations CVPT, RGE, and WCL shown in Figure 1. Turbidity data were downloaded from California Data Exchange Center gages inside Clifton Court Forebay (gage: CLC), at the confluence of Grant Line Canal and Old River (gage: GLC), and at Old River at Highway 4 (gage: OH4).

https://doi.org/10.15447/sfews.2026v24iss3art4

occurred in Old River in 2010, 2011, 2013, and 2017, and in Grant Line Canal in 2011 and 2014.

Telemetry Data in the WPA

A total of 1,066 juvenile Chinook Salmon were detected in the WPA; however, only 839 had a minimum of two detection events and thus were retained for analysis. Most study fish (823 of 839) were detected in 2010, 2011, 2013, or 2017—years when the rock barrier was not installed at HOR (Table 1). The majority (15 of 16) of the remaining study fish appear to have entered Old River through the rock barrier culvert (2012, 2014, and 2016). Although two fish were detected in the WPA in 2015, these fish were removed from the analysis since they each only had one detection event.

The 839 study fish made a total of 745 observed transitions (also referred to as "movements") between states, an average of < 1 movement per fish (Table 3). This pattern can occur if all detection events for some fish occur at only a single hydrophone array. There were many observations of fish leaving and returning to the same state (italicized numbers in Table 3), indicating that a fish left the detection range of the hydrophone array and then returned without first having been detected at another location. Of the 745 transitions between states, nine were compound movements that were not represented directly in the multi-state model (shown as underlined numbers in Table 3). For example, to account for the six observed transitions from RGE to CVPS, the fish movement model assumes that the fish passed through CVPT but were not detected there (Figure 2). Over 99% of movements between states (744 of 745) occurred within 5.4 days of first detection in the WPA, and one movement occurred after 9.2 days. The median time fish spent in the WPA was 32.8 hours (1.4 days).

The pattern of repeated detections at the same state was present even after predator-like detections were removed and the data were censored at 12 days. A total of 523 study fish (62%) triggered the predator filter and were likely predated after entering the WPA. Of these, 431 study fish (51.4%) were flagged by the predator filter for long residence time at a location, leaving uncertainty as to whether all predator-like detections had been removed. Despite the removal of all known predator-like detections from the detection histories, fish flagged as predated upon leaving a location (e.g., for long residence time) exhibited different patterns of observed transitions compared to the other study fish ($\chi^2 = 290.4$, $N = 2000$, simulated $p = 0.0005$).

Table 3 Observed juvenile Chinook Salmon movements in telemetry data in the WPA. Observations of fish leaving and returning to the same state are shown as *italicized* numbers; underlined numbers are observations of movements not allowed as direct transitions in the fish-movement model.

All study fish (n = 839)					
	To:				
From:	**1-CVPT**	**2-CVPS**	**3-RGE**	**4-CCFB**	**5-DS**
1-CVPT	*1795*	77	50	0	32
2-CVPS	0	0	0	0	0
3-RGE	65	6	*258*	311	98
4-CCFB	0	0	78	*4466*	0
5-DS	8	3	17	0	*1226*
Fish with detection histories that were censored at 12 days as a result of long residence time but that may still contain predator-like detections (LRCen.ind = 1; n = 431)					
	To:				
From:	**1-CVPT**	**2-CVPS**	**3-RGE**	**4-CCFB**	**5-DS**
1-CVPT	*1482*	0	29	0	5
2-CVPS	0	0	0	0	0
3-RGE	44	0	*188*	255	30
4-CCFB	0	0	74	*4246*	0
5-DS	2	0	13	0	*813*
Fish for which there is high confidence that only smolt-like detections remain in the detection histories (LRCen.ind = 0; n = 408)					
	To:				
From:	**1-CVPT**	**2-CVPS**	**3-RGE**	**4-CCFB**	**5-DS**
1-CVPT	*313*	77	21	0	23
2-CVPS	0	0	0	0	0
3-RGE	21	6	*70*	56	68
4-CCFB	0	0	4	*220*	0
5-DS	6	3	4	0	*413*

Fish Movement Analysis

Based on LR tests, all single covariate models were a significant improvement (at a 5% level) over the baseline indicator model, after correction

for multiple testing (LR ≥ 63, df = 8, $p < 0.001$; Table 4), indicating improved ability to explain juvenile Chinook Salmon movements in the WPA. No single variable resulted in an important effect (HR 95% CI excluding 1) on all movements. The single flow variable that accounted for the most variation in movement was net flow through the radial gates (Flow.RGE.net), which was associated with multiple movements, including between RGE and CCFB (3→4 and 4→3). However, the model that used the best local flow variable to model each transition ("Local Flow" model in Table 4) was superior to using only a single flow variable. The indicator for radial gates opening and closing (RG.ind) was associated with movements between RGE and CCFB, but this indicator performed less well than other flow and operations variables. The environmental variable most associated with movements was turbidity (Turb), with an important influence on movements between RGE and CCFB (3→4 and 4→3), from RGE to CVPT (3→1), and into CVPS (1→2). Models using water temperature and percent SJR water performed less well than the turbidity model, despite having an association with four to five movements each. The model with chlorophyll concentration did not converge to a solution. The model using fish fork length was the poorest-performing single-variable model.

Results from the single-variable models informed the set of multi-variable models that we then evaluated (Table 5). Our initial multi-variable model included local flow variables ("Local Flow" model in Table 4) and added turbidity because these were the best performing flow and operations and environmental variables in single-variable modeling. The full model added

Table 4 Single-variable modeling results compared to the baseline indicator model and effects on movement hazard ratios (HR). The number of observations of each movement (n_{Obs}) is shown at the bottom of each column.

Covariate[a]	Covariate Type	LR[b]	p	Movement HR Effect[c,d]							
				1→2	1→3	1→5	3→1	3→4	3→5	4→3	5→3
Local Flow[e]	Flow and Operations	851.5	< 0.001	–	+		–	–	+	+	–
Flow.RGE.net	Flow and Operations	567.1	< 0.001		+	+		–		+	+
Flow.RGE	Flow and Operations	433.5	< 0.001	–	+			–			
Flow.CVPT.net	Flow and Operations	377.1	< 0.001	–	+	+		–	+	+	
Flow.WCL.tdl	Flow and Operations	299.7	< 0.001		+	+	–		+		–
Flow.CVPT.tdl	Flow and Operations	247.2	< 0.001		+	+	–	+	+		–
RG.ind	Operations Indicator	188.6	< 0.001					+	–		+
Turb	Environmental	144.7	< 0.001	+			–	+		+	
SJRW.pct	Environmental	102.0	< 0.001					+	+	+	–
Temp.max	Environmental	92.8	< 0.001			–	+	+		–	+
Temp.mean	Environmental	90.0	< 0.001			–	+	+		–	+
Flow.WCL.net	Flow and Operations	86.0	< 0.001	–	+	+		–		+	–
Temp.cont	Environmental	72.4	< 0.001		–	–		+		–	+
Fish.length	Fish Characteristic	63.0	< 0.001			+	+	+			
			n_{Obs}	77	50	32	65	311	98	78	17

a. Covariates are defined in Table 2.
b. The LR was used as the $\chi 2$ test metric to compare single covariate models to the baseline (no covariate) model using a Chi-squared test (df = 8). All single covariate models were a significant improvement over the baseline model ($p < 0.001$).
c. HR effects are characterized as follows: "+" indicates that the HR and 95% CI are > 1, increasing the rate of a transition relative to the baseline model; "–" indicates that the HR and 95% CI are < 1, decreasing the rate of a transition; no symbol indicates that the HR and 95% CI include 1 and are therefore not important.
d. State transitions indicate numbered states as shown in Figure 2 and are as follows: 1-CVPT, 2-CVPS, 3-RGE, 4-CCFB, 5-DS. The transition from 5 to 1 was not fitted with covariates because only eight transitions were observed in the data.
e. The "Local Flow" model was constructed as follows: Flow.CVPT.net for transitions away from CVPT (1→2, 1→3, and 1→5), Flow.RGE.net for transitions into and out of CCFB (3 →4 and 4→3), and Flow.WCL.tdl for transitions away from RGE (3→1 and 3→5) and from DS to RGE (5→3).

https://doi.org/10.15447/sfews.2026v24iss3art4

the complementary component of flow (tidal, net, or radial gate indicator) for each transition. The best-performing model, determined by AICc, simplified the full model by dropping the turbidity variable from transitions where it was unimportant: CVPT to DS (1→5), RGE to CVPT (3→1), RGE to DS (3→5), and DS to RGE (5→3).

Estimates of the regression coefficients (i.e., log[HR]) for the best fitting multivariable model are shown in Figure 5. Results presented here are for fish that had a non-censored detection history and that were released at Durham Ferry because these results are most likely to represent the juvenile Chinook Salmon that migrate from upstream on the SJR. Model results related to the nuisance indicator variables LRcens.ind and OR.ind are presented in Appendix B.

The estimated baseline movement rates (i.e., rates without covariate effects) away from CVPT were low ($\hat{q}^0_{12}, \hat{q}^0_{13}, \hat{q}^0_{15}$, ≤0.01). The rate of fish movement from CVPT into CVPS (1→2) *decreased* when downstream-directed flow at CVPT (Flow.CVPT.net) increased, but *increased* at night (Night.ind = 1). The rate of fish movements downstream from CVPT to RGE (1→3) increased when flow at CVPT was less negative, and for positive tidal flow (i.e., ebb tides), and decreased at night. The rate of fish movement from both CVPT into CVPS (1→2) and CVPT to RGE (1→3) increased when there was high turbidity at the western end of Grant Line Canal (GLC gage). The rate of downstream movements from CVPT to DS (1→5) increased when flow at CVPT was less negative and for positive tidal flow (i.e., ebb tides).

For fish detected at RGE, the estimated baseline rates of movement upstream ($\hat{q}^0_{31} = 0.15$) or downstream ($\hat{q}^0_{35} = 0.013$) were much lower than the rate of movement to CCFB ($\hat{q}^0_{34} = 6.78$). The rate of upstream movement from RGE to CVPT (3→1) decreased under positive tidal flow in West Canal. The rate of fish movement from RGE to

Table 5 Results of multi-variable fish movement modeling. The total number of modeled parameters, k, includes the nine baseline movement-rate parameters. Models were ranked based on difference (**Δ**) from the lowest small sample size corrected Akaike Information Criteria (AICc) score.

Model Description	Movement[a]	Covariates[b]	k	ΔAICc
Baseline Indicators + Local Flow + Best Environmental + Additional Flow & Operation Components (Simplified Model)	1→2 1→3 1→5 3→1 3→4 3→5 4→3 5→3	LRCen.ind + Night.ind + OR.ind + Flow.CVPT.net + Flow.CVPT.tdl + Turb LRCen.ind + Night.ind + OR.ind + Flow.CVPT.net + Flow.CVPT.tdl + Turb LRCen.ind + Flow.CVPT.net + Flow.CVPT.tdl LRCen.ind + Night.ind + OR.ind + Flow.WCL.tdl + Flow.WCL.net LRCen.ind + Night.ind + OR.ind + Flow.RGE.net + RG.ind + Turb LRCen.ind + OR.ind + Flow.WCL.tdl + Flow.WCL.net LRCen.ind + Night.ind + OR.ind + Flow.RGE.net + RG.ind + Turb LRCen.ind + OR.ind + Flow.WCL.tdl + Flow.WCL.net	49	0
Baseline Indicators + Local Flow + Best Environmental + Additional Flow & Operation Components (Full Model)	1→2 1→3 1→5 3→1 3→4 3→5 4→3 5→3	LRCen.ind + Night.ind + OR.ind + Flow.CVPT.net + Flow.CVPT.tdl + Turb LRCen.ind + Night.ind + OR.ind + Flow.CVPT.net + Flow.CVPT.tdl + Turb LRCen.ind + Flow.CVPT.net + Flow.CVPT.tdl + Turb LRCen.ind + Night.ind + OR.ind + Flow.WCL.tdl + Flow.WCL.net + Turb LRCen.ind + Night.ind + OR.ind + Flow.RGE.net + RG.ind + Turb LRCen.ind + OR.ind + Flow.WCL.tdl + Flow.WCL.net + Turb LRCen.ind + Night.ind + OR.ind + Flow.RGE.net + RG.ind + Turb LRCen.ind + OR.ind + Flow.WCL.tdl + Flow.WCL.net + Turb	53	2.6
Baseline Indicators + Local Flow + Best Environmental (Initial Model)	1→2 1→3 1→5 3→1 3→4 3→5 4→3 5→3	LRCen.ind + Night.ind + OR.ind + Flow.CVPT.net + Turb LRCen.ind + Night.ind + OR.ind + Flow.CVPT.net + Turb LRCen.ind + Flow.CVPT.net + Turb LRCen.ind + Night.ind + OR.ind + Flow.WCL.tdl + Turb LRCen.ind + Night.ind + OR.ind + Flow.RGE.net + Turb LRCen.ind + OR.ind + Flow.WCL.tdl + Turb LRCen.ind + Night.ind + OR.ind + Flow.RGE.net + Turb LRCen.ind + OR.ind + Flow.WCL.tdl + Turb	45	101.4

a. Arrows indicate the direction of state movement using state numbers defined in Figure 2.
b. Model covariates are defined in Table 2.

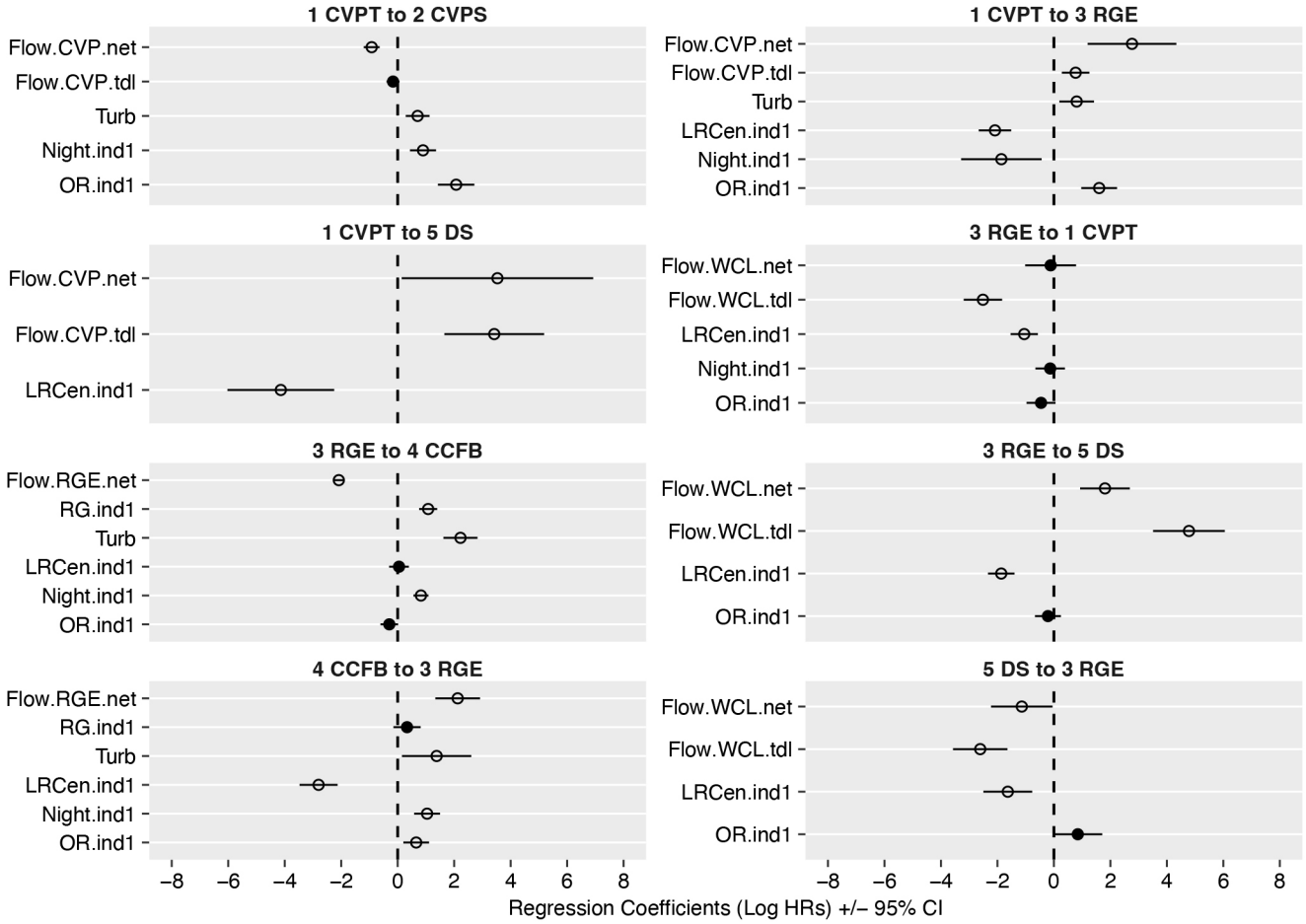

Figure 5 Estimated regression coefficients for the best multi-variable model. Important variable effects were those for which the regression coefficient point estimate (shown as *open circles*) and 95% CIs do not include zero. The indicator LRCen.ind1 had a decreasing effect (i.e., negative coefficient) on 1 CVPT to 2 CVPS but is omitted for figure clarity because of wide CIs. Non-important regression coefficients are shown as *solid black dots*. Regression coefficients are β = log(HR).

DS (3→5) increased with increasing downstream-directed (i.e., less negative) net and tidal flow in West Canal (Flow.WCL.net and Flow.WCL.tdl).

The estimated baseline rate of upstream movement from DS to RGE ($\hat{q}^0_{53} = 0.013$) was approximately equal to the baseline rate of fish moving in the opposite direction. The rate of fish moving from DS to RGE (5→3) decreased with increasing downstream-directed net and tidal flow (i.e., ebb tide) in West Canal.

The estimated baseline rate of fish moving from RGE to CCFB ($\hat{q}^0_{34} = 6.78$) was >100 times higher than the baseline rate of fish moving from CCFB to RGE ($\hat{q}^0_{43} = 0.053$). The rate of fish movement from RGE to CCFB (3→4) decreased when there was less negative net flow into Clifton Court Forebay (Flow.RGE.net), and increased when the radial gates were open, when turbidity increased in CCFB (CLC gage), and at night. The movement rate from CCFB to RGE (4→3) increased when there was less negative net flow into Clifton Court Forebay, when turbidity increased, and at night.

Transition Probabilities (1 Hour)

The predicted probability that a fish detected at one state would be detected at another state after time t = 1 hour varied, depending on flow and turbidity conditions in the WPA and on time

https://doi.org/10.15447/sfews.2026v24iss3art4

of day. While fish were in the WPA, net flow at CVPT (Flow.CVPT.net) ranged from –122.6 to 23.3 $m^3 s^{-1}$, and tidal flow at CVPT (Flow.CVPT.tdl) ranged from –16.6 to 16.5 $m^3 s^{-1}$. The predicted probability of moving from CVPT to CVPS (1→2) was approximately 2.5 times higher at night and ranged from 0.11 at the most negative net flow to < 0.013 at the least negative net flow at night (Figure 6A). The effect of tidal flow on the predicted probability of moving from CVPT to CVPS (1→2) was small (maximum: 0.01), but the predicted probability of this movement was approximately 20 times higher on the most negative flood tide flow (–16.6 $m^3 s^{-1}$) compared to the most positive ebb tide flow (16.5 $m^3 s^{-1}$). Compared to movements from CVPT to CVPS (1→2), the predicted probability of moving from CVPT to RGE (1→3) was much lower: when net flow at CVPT was the least negative (–23.3 $m^3 s^{-1}$) and when tidal flow was most positive, the predicted probability of fish moving from CVPT to RGE (1→3) was approximately 0.01. During high turbidity, the predicted probability of moving from CVPT to CVPS (1→2) increased up to 0.84 at night, and the predicted probability of moving from CVPT to RGE (1→3) increased up to 0.51 during the day, but there was high uncertainty associated with both estimates because transient high-turbidity events were not well represented in the data (Figure 7A). The predicted 1-hour probability of fish moving from CVPT to DS (1→5) was generally very low (< 1.8e-04) but increased to 1.0 when tidal flow was most positive, although there was high uncertainty (Figure 6B).

While fish were in the WPA, tidal flow at WCL (Flow.WCL.tdl) ranged from –351.5 to 278.9 $m^3 s^{-1}$, and net flow (Flow.WCL.net) ranged from –151 to 167.6 $m^3 s^{-1}$. The predicted probability of fish moving from RGE to CVPT (3→1), RGE to DS (3→5), or DS to RGE (5→3) over a 1-hour period was more strongly influenced by tidal flow than by net flow in West Canal (WCL; Figure 6C). The predicted probability of fish moving downstream from RGE to DS (3→5) varied from near zero on all negative flood tides and low positive tides up to 1.00 on the most positive ebb tide. The predicted probability of fish moving upstream from RGE to CVPT (3→1) varied from near zero on the most positive ebb tide and low negative flood tides up to 0.94 on the most negative flood tide. The estimated probability of upstream movement from DS to RGE (5→3) varied from near zero on all positive ebb tides and negative flood tides less than approximately –150 $m^3 s^{-1}$, but increased to a maximum of 0.13 at flood tides of approximately –325 $m^3 s^{-1}$.

Net flow through the radial gates into Clifton Court Forebay (Flow.RGE.net) ranged from –212 to 0 $m^3 s^{-1}$ while fish were in the WPA. The predicted probability of fish moving from RGE to CCFB (3→4) exceeded 0.50 at net flow < –135 $m^3 s^{-1}$ at night and < –170 $m^3 s^{-1}$ during the day, and exceeded 0.85 at flows < 178 $m^3 s^{-1}$ at night and < 212 $m^3 s^{-1}$ during the day (Figure 6D). The predicted probability of fish moving from RGE to CCFB (3→4) increased 5 to 8 times as turbidity in CCFB doubled from 25 NTU to 50 NTU, and was higher at night (Figure 7B). The predicted probability of fish moving from CCFB to RGE (4→3) was < 0.10 regardless of time of day and net flow conditions, except under high turbidity, when the predicted probability of moving from CCFB to RGE increased up to approximately 0.18 at night (but with high uncertainty; Figure 7B).

Piecewise Transition Probabilities (3-Day)

Piecewise transition probabilities were predicted using the fitted multi-variable model for two 3-day periods: 18–20 June 2011 and 20–22 May 2013. Each transition probability represents the probability of detection at state *s* at a given time in the 3-day period, conditional on detection at state *r* at the start of the 3-day period.

- From **18–20 June 2011**, net flows were strongly negative, and a high-turbidity event occurred near CVPT (at the GLC gage; Table 6). SJR inflow was 281 to 287 $m^3 s^{-1}$ on these days, which was lower than the peak spring inflow of 809 $m^3 s^{-1}$ that occurred in April 2011 but higher than on the same days in all other years of the study except 2017. During this 3-day period of relatively high SJR inflow and reverse (i.e., negative) net flows, the predicted probability of all transitions was < 0.025 or had confidence intervals that included zero

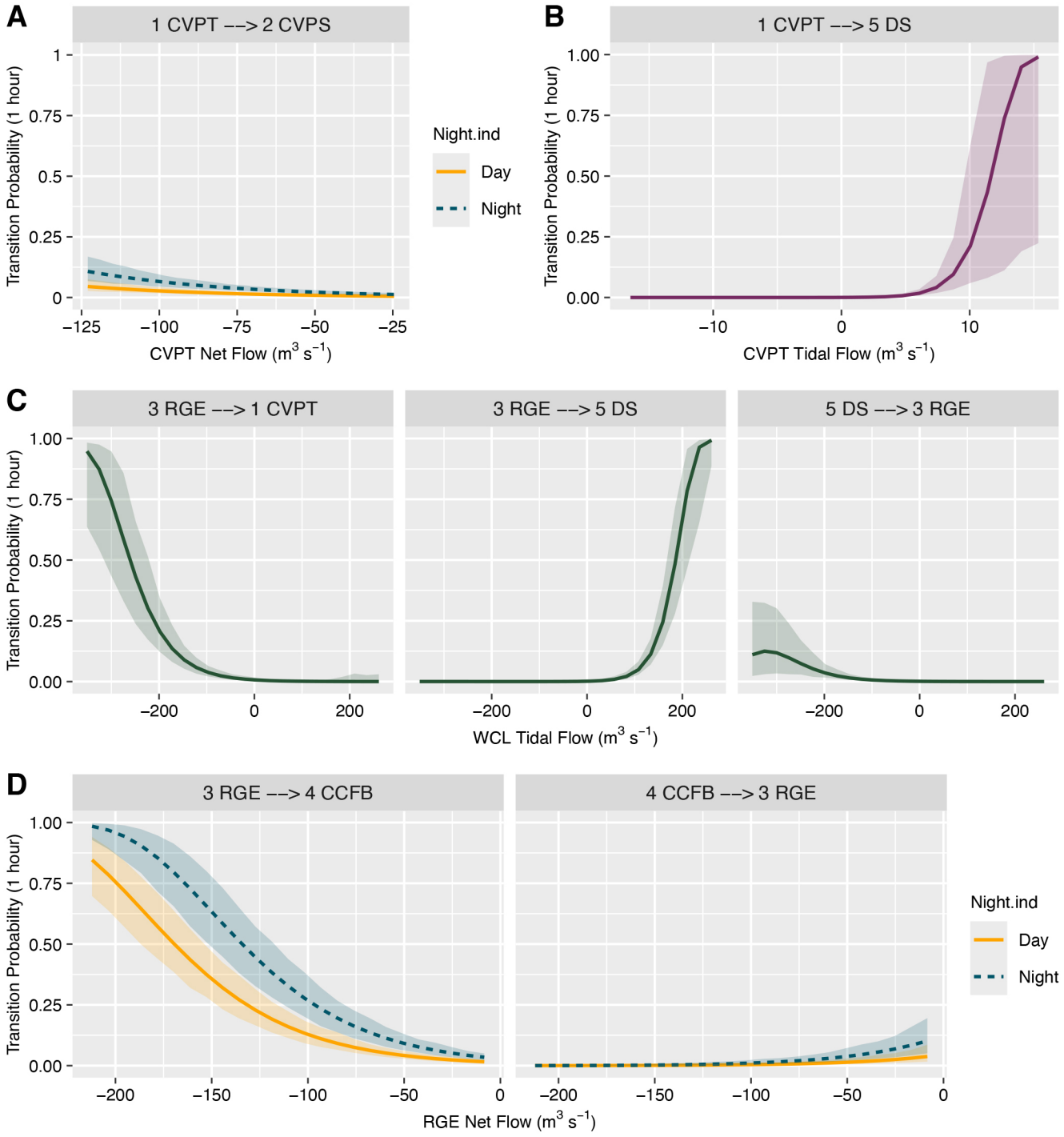

Figure 6 Predicted 1-hour transition probabilities for juvenile Chinook Salmon movements influenced by (**A**) CVPT Net Flow, (**B**) CVP Tidal Flow, (**C**) WCL Tidal Flow, and (**D**) RGE Net Flow. Movements and conditions not shown had 1-hour transition probabilities close to zero.

https://doi.org/10.15447/sfews.2026v24iss3art4

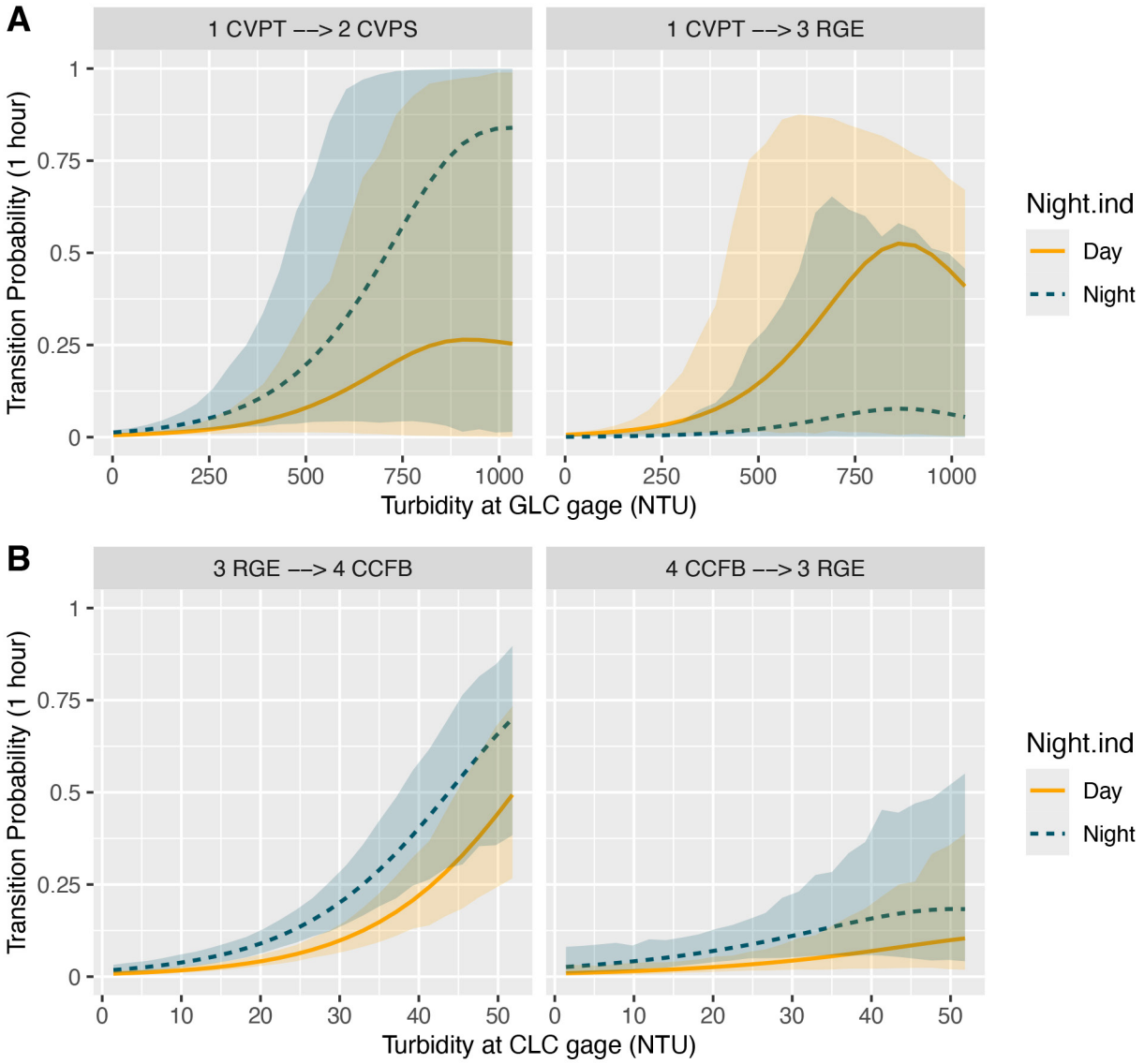

Figure 7 Predicted 1-hour transition probabilities for juvenile Chinook Salmon movements influenced by turbidity at (**A**) GLC and (**B**) CLC.

throughout the 3-day period except for CVPT to CVPS (1→2), RGE to CCFB (3→4), and DS to CCFB (5→4). The predicted probability of a fish detected at 3 RGE later being detected at 4 CCFB was >0.99 throughout this 3-day period. Additionally, the predicted probability of a fish detected at 5 DS later being detected at 4 CCFB increased to 0.76 after 3 days; however, there was high uncertainty associated with this transition (Figure 8A). The probability of a fish detected at 1 CVPT later being detected at 2 CVPS increased to >0.95 after approximately 17 hours (0.7 day).

- From **20–22 May 2013**, the magnitude of the net flow was less negative compared to 2011 and turbidity was lower (Table 6). SJR inflow ranged from 30.2 to 36.3 $m^3 s^{-1}$ on these days, which was lower than the peak spring inflow of 118 $m^3 s^{-1}$ that occurred in early May 2013. During this period of low SJR inflow and low reversed flows, there were more transitions with a predicted probability >0.025 than

under the high flow 2011 conditions, but no single transition dominated during the 3 days (Figures 8B, 8C, and 8D). The predicted probability of eventually transitioning from 1 CVPT, 3 RGE, or 5 DS to 2 CVPS increased nearly linearly and reached 0.46, 0.33, and 0.12, respectively, after 3 days. Under the low flow conditions of 2013, the influence of tidal flow was stronger, corresponding to "waves" in the transition probabilities. For example, the predicted probability of transition from 1 CVPT to 5 DS increased to 0.35 over the 3 days (Figure 8B) but also varied cyclically with the tides. For fish detected at 3 RGE, the probability of later being detected at 1 CVPT peaked at 0.50 after approximately 3 hours in the WPA and then declined to 0.15 after 3 days, the probability of later being detected at 4 CCFB increased to 0.25 after 0.25 days but then declined, and the probability of later

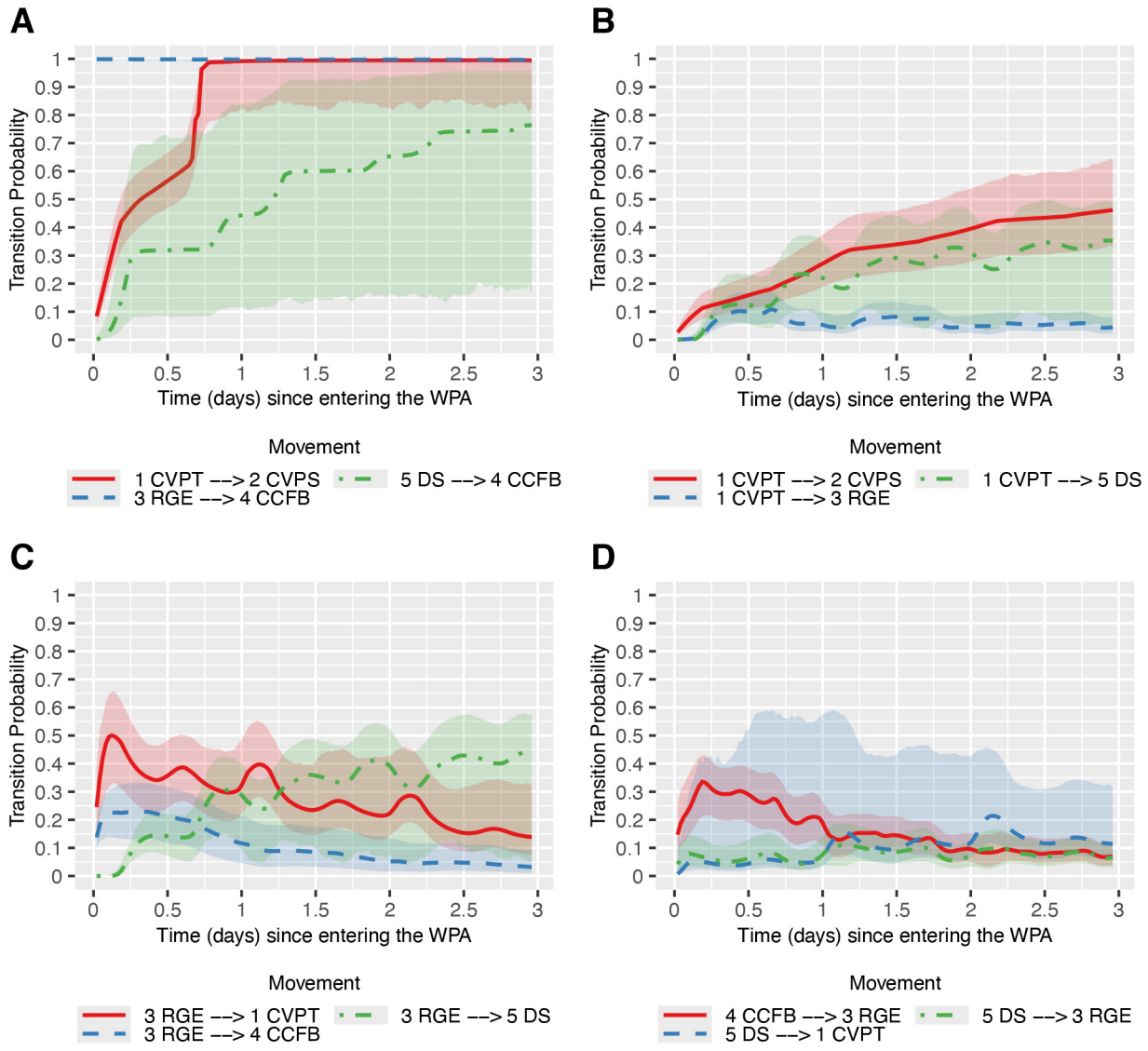

Figure 8 Predicted 3-day transition probabilities for juvenile Chinook Salmon under variable water year conditions. Transition probabilities represent the probability of detection at state *s* at a given time conditional on detection at state *r* at the start of the 3-day period; time is assumed to start at midnight on the first day of the 3-day period. In a wet water year (**A**; 18 to 20 June 2011), only the transitions shown had predicted probabilities that were at least 0.025 (2.5%) during the 3-day period. In a critical water year (**B**, **C**, and **D**; 20 to 22 May 2013), the probability of transitions to 2 CVPS or 4 CCFB (i.e., entrainment) were lower compared to the wet water year period, and other transition probabilities were higher.

https://doi.org/10.15447/sfews.2026v24iss3art4

being detected at 5 DS peaked at 0.45 after 3 days (Figure 8C). In general, the predicted probability of upstream transitions from 5 DS to 3 RGE or 1 CVPT was low (< 0.21) under the low reverse flow conditions in 2013 (Figure 8D). Additionally, under 2013 conditions, fish detected at 4 CCFB had a higher probability of later being detected elsewhere (e.g. 4 CCFB→3 RGE, shown in Figure 8D) compared to high reverse net flow conditions in 2011 when the probability of transition away from 4 CCFB was near zero.

DISCUSSION

We identified several key findings in our analysis of juvenile Chinook Salmon movements in the WPA of the South Delta:

1. Flow conditions in the WPA are driven by both exports (i.e., negative net flow at CVPT and RGE) and tidal fluctuations—and both strongly influenced juvenile Chinook Salmon movement patterns.

2. Juvenile Chinook Salmon movements in West Canal between Highway 4 and the radial gates were influenced by tidal flow and, to a lesser extent, net flow.

3. For fish at the CVP trash racks, the strongest effects on movement were from CVP net flow and time of day.

4. Export operations that resulted in negative net flow at CVPT and RGE drew juvenile Chinook Salmon into the water-export facilities when exports were high.

5. High predation of juvenile salmon complicated interpretation of fish movement in the WPA.

Both tidal flow and net flow influenced movements of juvenile Chinook Salmon in the WPA; which the more influential flow component was varied spatially. In the region between the radial gates (RGE) and the DS location comprising the acoustic receivers in West Canal (WCL) and at Highway 4 (OH4), movement of juvenile salmon was related most to tidal flow in West Canal. Juvenile salmon moved upstream toward RGE (5 DS→3 RGE) and from RGE toward the CVP trash racks (3 RGE→1 CVPT) on flood tides, and downstream from RGE (3 RGE→5 DS) on ebb tides. The probability of upstream movement from the radial gates to CVP (3 RGE→1 CVPT) was near zero during slack and ebb tides, but rapidly increased to >0.75 at the maximum flood tide of 351.5 $m^3 s^{-1}$, whereas the opposite relationship held true for the downstream movement (3 RGE→5 DS; Figure 6C). The finding that juvenile Chinook Salmon movements in the WPA "went with the flow" of the twice daily ebb and flood tides was consistent with other studies of juvenile salmonids in tidally influenced habitats (Chapman et al. 2009; Hering et al. 2010; Anchor QEA 2022; Dodrill et al. 2022; Buchanan 2024).

For fish at the CVPT, movements were generally more influenced by net flow than by tidal flow. More fish entering CVP salvage (1 CVPT→2 CVPS) under increased negative net flow (i.e., higher CVP exports) and more fish moving downstream to RGE (1 CVPT→3 RGE) under increased positive net flow (Figure 5). The lower sensitivity of fish movements to tidal flow at CVPT may reflect the influence of a longer input channel connecting CVPT to Old River, resulting in a lower magnitude of tidal flow. By comparison, the higher sensitivity fish movements to tidal flow at RGE may reflect the short channel connecting RGE to to West Canal, where tidal flow magnitude is higher (Figure 3). However, the number of fish moving downstream from CVPT (1 CVPT→5 DS) increased during ebb tides (Figure 6B), likely because the tidal flow variations at CVPT corresponded to higher downstream flow once fish reached West Canal.

Within the WPA, higher export flow (i.e., more negative net flow at CVPT and at RGE) increased the chance of juvenile Chinook Salmon entering the facilities over a 1-hour period (Figure 6A and 6D). Net flow in West Canal had a lower effect on fish movements at either WCL or OH4. By comparison, net flow in West Canal had a much

lower effect on fish movements. Higher West Canal net flow—which can occur when export operations are lower or SJR inflow is higher—was only associated with a small increase (from near 0 to 0.02) in the probability of movement from the radial gates to downstream in the Delta (3 RGE→5 DS) near the highest positive net flow of 168 $m^3 s^{-1}$. Comparing a relatively high flow and high pumping period (18 to 20 June 2011) with a relatively low flow and low pumping period (20 to 22 May 2013) through predicted 3-day piecewise transition probabilities highlights the interplay between exports and tidal influences (Figure 7). These two time-periods experienced similar magnitudes of tidal flow variations in West Canal (Table 6). At higher levels of pumping, fish were highly likely to enter either CVP salvage or Clifton Court Forebay—regardless of starting location—and therefore had low probability of having moved downstream by the end of 3 days. The effects of tidal flow were more pronounced during 20 to 22 May 2013, when both flows and pumping rates were lower, resulting in twice daily "bumps" in the transition probabilities and an increased chance of fish being detected at a location other than the CVP salvage or Clifton Court Forebay after 3 days. These model-based results support the idea that fish respond to localized flow forces that are driven by tidal flow during low net flow/low pumping conditions.

We found that some combinations of exports, tidal flow, and opening the radial gates at Clifton Court Forebay—which are designed to be opened at flood tides—increased the risk of entraining those juvenile Chinook Salmon that had previously passed downstream of the radial gate entrance channel. This occurs first by the flood tide pushing them back up-river to the radial gate entrance channel, and then by the export flow into Clifton Court Forebay drawing them into the forebay, resulting in delayed migration, predation risk within the forebay, and risk of entrainment in the pumps and water-conveyance canals (Gingras 1997; Kimmerer 2008; Grimaldo et al. 2009; NMFS 2009). Based on the movement patterns observed in these data, restrictions in exports during the spring emigration are expected to limit fish in the WPA from entering either the CVP or Clifton Court Forebay. However, export restrictions may not increase survival of SJR-origin fall-run Chinook Salmon entrained into the CVP because most acoustic-tagged fish surviving to Chipps Island were first salvaged and then transported to downstream release sites (Buchanan, Barnard, and Brandes 2018). On the other hand—and assuming that other native fish species respond to local flow signals similarly to fall-run Chinook Salmon—survival benefits of avoiding the facilities may accrue to spring-run Chinook Salmon, juvenile Chinook Salmon from the Sacramento River, and Delta Smelt, for which regional survival patterns differ (Chinook Salmon: Hance et al. 2022; Hause et al. 2022) or for which facility survival is expected to be particularly low (Delta Smelt: Grimaldo et al. 2009).

Entry of juvenile Chinook Salmon into the water export facilities was related to time of day and turbidity as well as to export flow. At both the CVP trash racks and the radial gates, juvenile salmon were more likely to enter the facility (CVPS or CCFB model states, respectively) if they arrived at night rather than in the daytime.

Table 6 Environmental conditions in the water project area (WPA) used to calculate 3-day transition probabilities

Covariate	Unit	Median	Mean	Min	Max
18–20 June 2011 (Wet Water Year Type)					
Flow.RGE.net	$m^3 s^{-1}$	−194.1	−194.8	−201.1	−186.4
Flow.CVPT.net	$m^3 s^{-1}$	−85.6	−85.7	−85.8	−85.5
Flow.CVPT.tdl	$m^3 s^{-1}$	−1.5	−0.25	−8.4	9.8
Flow.WCL.net	$m^3 s^{-1}$	−113.7	−114.7	−119.7	−110.9
Flow.WCL.tdl	m3 s-1	24.9	−0.43	−195.3	216.2
Turb (GLC)	NTU	64.4	199.1	12.5	1064
Turb (CLC)	NTU	23.6	23.4	17.2	29.4
20–22 May 2013 (Critical Water Year Type)					
Flow.RGE.net	$m^3 s^{-1}$	−19.0	−19.0	−20.0	−17.8
Flow.CVPT.net	$m^3 s^{-1}$	−23.8	-23.8	−23.9	−23.7
Flow.CVPT.tdl	$m^3 s^{-1}$	0.82	0.10	v6.3	6.7
Flow.WCL.net	$m^3 s^{-1}$	−28.3	-28.5	−31.8	-24.8
Flow.WCL.tdl	$m^3 s^{-1}$	25.9	1.4	−205.9	145.0
Turb (GLC)	NTU	7.9	8.6	5.2	20.3
Turb (CLC)	NTU	20.1	23.2	10.7	76.9

https://doi.org/10.15447/sfews.2026v24iss3art4

Conversely, the probability of juvenile salmon moving downstream from the CVP trash racks to the radial gates (1 CVPT→3 RGE) was higher during the day. The higher probability of their entering the facility at night may reflect increased predator avoidance behavior because out-migrating juvenile salmon use nocturnal migration as a strategy to reduce predation risk (Chapman et al. 2013; Clark et al. 2016; Furey et al. 2016), especially at smaller sizes (Ibbotson et al. 2011). While the hatchery-origin fish used in this study were larger than natural-origin Chinook Salmon out-migrating through the system at the same time, they were small (73 to 140 mm) compared to concurrently released hatchery-origin SJR steelhead (97 to 396 mm; Buchanan et al. 2021), and likely would be preferentially preyed on, relative to the larger steelhead (Michel et al. 2018). The higher probability of daytime movement away from the CVP may reflect imperfect holding (e.g., drifting) or may relate to the presence of the trash racks themselves, which may attract visual predators and thus influence diel movement patterns of juvenile salmonids (Grossman 2016; Smith et al. 2021). The higher probability of fish entering the facility during high-turbidity events may also reflect predator avoidance (Gregory and Levings 1998) or, conversely, avoidance of potentially physiologically detrimental conditions (Bash et al. 2001; Lehman et al. 2017).

Modeling and interpreting fish movement patterns from acoustic telemetry data in the WPA was challenging because of the high predation risk in this area (Grossman 2016). Over 60% (523 of 839) of the tagged juvenile Chinook Salmon that met the detection criteria for inclusion in this analysis triggered the predator filter after entering the WPA. This is consistent with prior identification of the CVP trash racks and Clifton Court Forebay entrance as known hotspots of introduced predatory fish, including Largemouth Bass (*Micropterus nigricans*) and Striped Bass (*Morone saxatilis*; Vogel 2011; Grossman 2016). Applying the predator filter to the data increased the likelihood that only smolt-like detections remained in the dataset. For time-to-event analyses such as that those used in this study, the predator filter is particularly effective when it is triggered in response to behavior during a transition (e.g., movement against the local flow direction or extreme movement speed; Vogel 2011; Buchanan and Whitlock 2022a) but is less effective when it is triggered by long residence time in a single location. In the first case, all detections at the new location are removed and all prior detections can be considered smolt-like. In the second case, the predator designation is assigned at the end of the detection event, and there is uncertainty about when during the long detection event the predation occurred. We accounted for the uncertainty in the predation event timing by modeling the effect of long residence time on movement patterns of fish with triggered tags. We observed the largest effects for movements from the CVP trash racks to either CVP salvage (1 CVPT→2 CVPS) or the West Canal/Highway 4 receivers (1 CVPT→5 DS), and from Clifton Court Forebay to the radial gates entrance (4 CCFB→3 RGE). Compared to other fish in the dataset, those with long residence times accumulated a higher number of repeated detections at CVPT and CCFB, and these two locations were where 80% of the fish that had triggered tags were last detected. The repeated detections likely represented predator "lurking" behavior, indicating that some predator detections remained in the dataset even after the predator filter.

Despite modeling challenges that arose from uncertainty in predator diagnosis and limitations in both sample size and replication of inflow and operational conditions, our analysis of these telemetry data—collected over nearly 10 years of field study—contributes to existing understanding of the effects of water management on SJR-origin juvenile Chinook Salmon movement and survival patterns in the Delta (Buchanan et al. 2013; Buchanan, Brandes, and Ingram 2018; SST 2017a; Buchanan and Skalski 2020; Buchanan and Whitlock 2022b; Dodrill et al. 2022; and Wohner et al. 2022). Over this period, which ranged from hydrologically wet (2011, 2017) to critically dry (2013 to 2015), survival of SJR-origin fall-run juvenile Chinook Salmon through the Delta ranged from 0% to 11%, despite high SJR inflow in some years, and regardless of whether fish took

the interior Delta migration route via Old River or remained in the SJR mainstem (Buchanan, Brandes, and Ingram 2018). Nevertheless, survival patterns of SJR-origin Chinook Salmon are spatially variable (SST 2017b). Survival of juvenile salmonids in the more riverine regions of the Delta appears related to Delta inflow and temperature, while survival in the more tidal reaches has been consistently low (Buchanan, Brandes, and Ingram 2018). On a smaller scale, this analysis also observed spatial heterogeneity in movement factors within the WPA, with tidal flow more important in the West Canal north of Clifton Court Forebay entrance channel and for the upstream movement from the entrance channel to the CVP trash racks, but with net flow associated with pumping operations more important closer to the radial gates and the CVP trash racks (i.e., movements into the forebay and into CVP salvage; Figure 6).

CONCLUSION

Spatial variability in movement and survival factors means there are no simple levers to pull to significantly improve survival in the Delta for juvenile Chinook Salmon, but studies such as ours can help provide more detailed information on how localized environmental and flow conditions affect them in specific sub-areas of the Delta, such as the WPA. Potential management actions can be evaluated by integrating models focused on Delta sub-areas with spatially explicit Delta-wide models such as ECO-PTM, a particle-based model that applies salmon swimming and routing behaviors to particle "fish" to evaluate survival outcomes (Wang et al. 2024). This model has previously been developed with a focus on the North Delta and Sacramento River runs of salmon; a South Delta-focused version of ECO-PTM is currently in development (Wang et al. 2024). The South Delta ECO-PTM incorporates findings on juvenile Chinook Salmon movements from continuoustime multi-state models at key junctions on the SJR mainstem (Dodrill et al. 2022)—the same type of model we implemented in this study of Chinook Salmon movements near the water project facilities. Our study will help inform management of Chinook Salmon and increase understanding of the major factors that drive smolt movements within the WPA of the interior Delta. Our results may also be able to inform Delta-wide modelsthat managers can then use to evaluate suites of actions such as water operations, habitat restoration, increased flow, invasive vegetation removal, and how barrier installations affect survival outcomes. The multi-state movement modeling approach used here complements existing survival models and particle-tracking models as important tools for understanding salmon migration dynamics in this complex region. All available analytical tools should be used to help identify and monitor mechanisms that improve the survival of out-migrating salmonids in the highly complex and variable Delta.

ACKNOWLEDGMENTS

This project was conducted under State Water Contractors (SWC) 2023 Science Plan Grant funding, under Agreement 24-13. Linda Standlee (SWC) was the contracting liaison and Darcy Austin (SWC) was the science liaison for this project. We'd like to acknowledge Michelle Havey and Emma Nordlund for their assistance, support, and contributions to this project. Thank you to our reviewers for their thoughtful comments, which have made this a much better document.

REFERENCES

Anchor QEA. 2022. Synthesis of juvenile steelhead responses to hydrodynamic conditions in the Sacramento–San Joaquin Delta. Proposition 1 Delta Stewardship Council Contract Award 18203. Prepared for Delta Stewardship Council and State Water Contractors. April 2022. Available from: *https://sciencetracker.deltacouncil.ca.gov/activities/evaluating-juvenile-salmonid-behavioral-responses-hydrodynamic-conditions-sacramento-san*

Azat J, Killam D. 2024. GrandTab 2024.05.20 California Central Valley Chinook escapement database report. California Department of Fish and Wildlife. [accessed 2024 Oct 10]. Available from: *https://www.calfish.org/ProgramsData/Species/CDFWAnadromousResourceAssessment.aspx*

https://doi.org/10.15447/sfews.2026v24iss3art4

Barnard D, Brandes P, LaPlante D, Nichols K, Buchanan R, Israel J. 2022. 2016 South Delta Chinook Salmon survival study. Brandes P, Matthias B, editors. 20 April 2022. [accessed 2024 Sep 9]. Available from: *https://www.researchgate.net/publication/360074207_2016_South_Delta_Chinook_Salmon_Tagging_Study_DRAFT_REPORT*

Bash J, Berman C, Bolton S. 2001. Effects of turbidity and suspended solids on salmonids. Seattle (WA): University of Washington, Center for Streamside Studies. November 2021. [accessed 2025 Feb 20]. 80 p. Available from: *https://digital.lib.washington.edu/server/api/core/bitstreams/fd7b4f43-378c-45ea-8f6d-05ad19adf1bd/content*

Buchanan R, Barnard D, Brandes P, Towne K, Ingram J, Nichols K, LaPlante D, Israel J. 2018. 2015 South Delta Chinook Salmon survival study. [accessed 2024 Sep 9]. 16 April 2018. Available from: *https://www.researchgate.net/publication/359831748_2015_South_Delta_Chinook_Salmon_Tagging_Study*

Buchanan R, Brandes P, Ingram J, Marshall M, Nichols K, LaPlante D, Barnard D, Towne K, Israel J. 2018. 2014 South Delta Chinook Salmon survival study. 11 April 2018. [accessed 2024 April 4]. Available from: *https://www.researchgate.net/profile/Rebecca-Buchanan-4/publication/359831510_2014_South_Delta_Chinook_Salmon_Tagging_Study/links/6250b6a24f88c3119cea309f/2014-South-Delta-Chinook-Salmon-Tagging-Study.pdf*

Buchanan RA. 2024. Route use of emigrating steelhead in a heavily modified river delta. N Am J Fish Manag. [accessed 2024 Jun 26];44:714–734. *https://doi.org/10.1002/nafm.11005*

Buchanan RA, Brandes P, Marshall M, Foott JS, LaPlante D, Israel J. 2015. 2012 South Delta Chinook Salmon survival study. [accessed 2024 Sep 9]. 145 p. Available from: *https://www.noaa.gov/sites/default/files/legacy/document/2020/Oct/0.7.115.8842-000001.pdf*

Buchanan RA, Brandes P, Marshall M, Nichols K, Ingram J, LaPlante D, Israel J. 2016. 2013 South Delta Chinook Salmon survival study. 22 December. [accessed 2024 Sep 9]. Available from: *https://www.noaa.gov/sites/default/files/legacy/document/2020/Oct/0.7.115.8844-000001.pdf*

Buchanan RA, Brandes PL, Skalski JR. 2018a. Survival of juvenile fall-run Chinook Salmon through the San Joaquin River Delta, California, 2010–2015. N Am J Fish Manag. [accessed 2023 Mar 9];38:663–679. *https://doi.org/10.1002/nafm.10063*

Buchanan RA, Skalski JR. 2020. Relating survival of fall-run Chinook Salmon through the San Joaquin Delta to river flow. Environ Biol Fishes. [accessed 2024 Oct 21];103:389–410. *https://doi.org/10.1007/s10641-019-00918-y*

Buchanan RA, Skalski JR, Brandes PL, Fuller A. 2013. Route use and survival of juvenile Chinook salmon through the San Joaquin River Delta. N Am J Fish Manag. [accessed 2024 Mar 18];33:216–229. *https://doi.org/10.1080/02755947.2012.728178*

Buchanan RA, Buttermore E, Israel J. 2021. Outmigration survival of a threatened steelhead population through a tidal estuary. Can J Fish Aquat. Sci. [accessed 2024 Oct 30];78:1869–1886. *https://doi.org/10.1139/cjfas-2020-0467*

Buchanan RA, Whitlock SL. 2022a. Diagnosing predated tags in telemetry survival studies of migratory fishes in river systems. Anim Biotelemetry. [accessed 2025 Jan 8];10(13). *https://doi.org/10.1186/s40317-022-00283-1*

Buchanan RA, Whitlock SL. 2022b Understanding salmon migration dynamics in a datalimited environment. N Am J Fish Manag. [accessed 2023 Mar 14];42(5)1111–1113. *https://doi.org/10.1002/nafm.10799*

Burnham KP, Anderson DR. 2002. Model selection and multimodel inference. 2nd ed. [New York (NY): Springer. 488 p.

CBR (Columbia Basin Research, University of Washington), 2024. SacPAS CDFW GrandTab adult escapement. [accessed 2024 Oct 10]. Available from: *www.cbr.washington.edu/sacramento/data/query_adult_grandtab.html*

[CDWR] California Department of Water Resources. c2023. Spring head of Old River installation and removal dates. Sacramento (CA): CDWR. [accessed 2025 Feb 12]. Available from: *https://water.ca.gov/Programs/State-Water-Project/Operations-and-Maintenance/South-Delta-Temporary-Barriers-Project*

[CDWR] California Department of Water Resources. c2024. California Data Exchange Center. Sacramento (CA): CDWR. [accessed 2024 Mar 1]. Available from: *https://cdec.water.ca.gov/queryTools.html*

[CDWR] California Department of Water Resources. c2025a. California Data Exchange Center. Sacramento (CA): CDWR. [accessed 2025 Jan 15]. Available from: *https://cdec.water.ca.gov/queryTools.html*

[CDWR] California Department of Water Resources. c2025b. Chronological reconstructed Sacramento and San Joaquin Valley water year hydrologic classification indices. Sacramento (CA): CDWR. [accessed 2025 Jan 15]. Available from: *https://cdec.water.ca.gov/reportapp/javareports?name=WSIHIST*

Chapman ED, Hearn AR, Buckhorn M, Klimley AP, Lacivita PE, Brostoff WN, Bremner AM. 2009. Juvenile salmonid outmigration and green sturgeon distribution in the San Francisco Estuary: 2008–2009. University of California Davis and US Army Corps of Engineers. p. 90. Available from: *https://www.spn.usace.army.mil/Portals/68/docs/Dredging/LMTS/S%20and%20S/3%20-%20Chapman%20et%20al%202009%20Salmonid%20outmigration%20report%2020110107.doc*

Chapman ED, Hearn AR, Michel CJ, Ammann AJ, Lindley ST, Thomas MJ, Sandstrom PT, Singer GP, Peterson ML, MacFarlane RB, et al. 2013. Diel movements of out-migrating Chinook Salmon (*Oncorhynchus tshawytscha*) and Steelhead Trout (*Oncorhynchus mykiss*) smolts in the Sacramento/San Joaquin watershed. Environ Biol Fishes. [accessed 2022 Mar 30];96:273–286. *https://doi.org/10.1007/s10641-012-0001-x*

Clark TD, Furey NB, Rechisky EL, Gale MK, Jeffries KM, Porter AD, Casselman MT, Lotto AG, Patterson DA, Cooke SJ, et al. 2016. Tracking wild sockeye salmon smolts to the ocean reveals distinct regions of nocturnal movement and high mortality. Ecol Appl. [accessed 2025 Feb 12];26(4):959–978. *https://doi.org/10.1890/15-0632*

Crozier LG, McClure MM, Beechie T, Bograd SJ, Boughton DA, Carr M, Cooney TD, Dunham JB, Green CM, Haltuch MA, et al. 2019. Climate vulnerability assessment for Pacific salmon and steelhead in the California Current Large Marine Ecosystem. PLoS One. [accessed 2024 Oct 10];14(7):e021771. *https://doi.org/10.1371/journal.pone.0217711*

Dodrill M, Perry R, Pope A, Wang X. 2022. Quantifying the effects of tides, river flow, and barriers on movements of Chinook Salmon smolts at junctions in the Sacramento–San Joaquin River Delta using multistate models. Environ Biol Fishes [accessed 2024 Apr 5];105:2065–2082. *https://doi.org/10.1007/s10641-022-01273-1*

[ESA and AECOM] Environmental Science Associates and AECOM Technical Services, Inc. 2018. Effect of the South Delta agricultural barriers on emigrating juvenile salmonids. Prepared for California Department of Water Resources, Bay–Delta Office. November 2018. Available from: *https://cawaterlibrary.net/document/effect-of-the-south-delta-agricultural-barriers-on-emigrating-juvenile-salmonids/*

Furey NB, Hinch SG, Bass AL, Middleton CT, Minke–Martin V, Lotto AG. 2016. Predator swamping reduces predation risk during nocturnal migration of juvenile salmon in a high mortality landscape. J Anim Ecol. [accessed 2025 Feb 12];85(4):948–959. *https://doi.org/10.1111/1365-2656.12528*

Gregory RS, Levings CD. 1998. Turbidity reduces predation on migrating juvenile Pacific salmon. Trans Am Fish Soc. [accessed 2021 Mar 16];127(2):275–285. *https://doi.org/10.1577/1548-8659(1998)127%3C0275:TRPOMJ%3E2.0.CO;2*

Gingras M. 1997. Mark/recapture experiments at Clifton Court Forebay to estimate pre-screening loss to entrained juvenile fishes: 1976–1993. Sacramento (CA): California Department of Fish and Game, Interagency Ecological Program. Technical Report 55. Available from: *https://cawaterlibrary.net/document/mark-recapture-experiments-at-clifton-court-forebay-to-estimate-pre-screening-loss-to-juvenile-fishes-1976-1993/*

https://doi.org/10.15447/sfews.2026v24iss3art4

Grimaldo LF, Sommer T, Van Ark N, Jones G, Holland E, Moyle PB, Herbold B, Smith P, 2009. Factors affecting fish entrainment into massive water diversions in a tidal freshwater estuary: can fish losses be managed? N Am J Fish Manag. [accessed 2025 May 2];29:1253–1270. *https://doi.org/10.1577/M08-062.1*

Grossman GD. 2016. Predation on fishes in the Sacramento–San Joaquin Delta: current knowledge and future directions. San Franc Estuary Watershed Sci. [accessed 2025 Jan 24];14(2). *https://doi.org/10.15447/sfews.2016v14iss2art8*

Hance DJ, Perry RW, Pope AC, Ammann AJ, Hassrick JL, Hansen G. 2022. From drought to deluge: spatiotemporal variation in migration routing, survival, travel time and floodplain use of an endangered migratory fish. Can J Fish Aquat Sci. [accessed 2022 Apr 12];79(3):410–428. *https://doi.org/10.1139/cjfas-2021-0042*

Hause CL, Singer GP, Buchanan RA, Cocherell DE, Fangue NA, Rypel AL. 2022. Survival of a threatened salmon is linked to spatial variability in river conditions. Can J Fish Aquat Sci. [accessed 2025 May 5];79:2056–2071. *https://doi.org/10.1139/cjfas-2021-0243*

Hering DK, Bottom DL, Prentice EF, Jones KK, Fleming IA. 2010. Tidal movements and residency of subyearling Chinook Salmon (*Oncorhynchus tshawytscha*) in an Oregon salt marsh channel. Can J Fish Aquat Sci. [accessed 2025 Jan 31];67(3):524–533. *https://doi.org/10.1139/F10-003*

Holleman RC, Gross ES, Thomas MJ, Rypel AL, Fangue NA, 2022. Swimming behavior of emigrating Chinook Salmon smolts. PLoS ONE. [accessed 2022 Jun 6];17(3):e0263972. *https://doi.org/10.1371/journal.pone.0263972*

Hurvich CM, Tsai C-L. 1989. Regression and time series model selection in small samples. Biometrika. [accessed 2024 Sep 12];76:297–307. *https://doi.org/10.2307/2336663*

Ibbotson AT, Beaumont WRC, Pinder AC. 2011. A size-dependent migration strategy in Atlantic Salmon smolts: Small smolts favour nocturnal migration. Environ Biol Fishes. [accessed 2022 Mar 16];92(2):151–157. *https://doi.org/10.1007/s10641-011-9824-0*

Jackson CH. 2011. Multi-state models for panel data: the 'msm' package for R. J Stat Softw. [accessed 2021 Nov 3];38(8):1–28. *https://doi.org/10.18637/jss.v038.i08*

Jackson CH. 2023. 'msm': Multi-State Markov and Hidden Markov Models in Continuous Time. (package for R). Version 1.7.1. 23 November 2023. [accessed 2024 May 27]. Available from: *https://cran.r-project.org/web/packages/msm/index.html*

Kimmerer WJ. 2008. Losses of Sacramento River Chinook Salmon and Delta Smelt to entrainment in water diversions in the Sacramento–San Joaquin Delta. San Franc Estuary Watershed Sci. [2016 May 4];6(2). *https://doi.org/10.15447/sfews.2008v6iss2art2*

Lehman B, Huff DD, Hayes SA, Lindley ST. 2017. Relationships between Chinook Salmon swimming performance and water quality in the San Joaquin River, California. Trans Am Fish Soc. [accessed 2024 Oct 21];146(2):349–358. *https://doi.org/10.1080/00028487.2016.1271827*

Luoma SN, Dahm CN, Healey M, Moore JN, 2015. Challenges facing the Sacramento–San Joaquin Delta: Complex, chaotic, or simply cantankerous? San Franc Estuary Watershed Sci. [accessed 2022 Mar 10];13(3). *https://doi.org/10.15447/sfews.2015v13iss3art7*

MacWilliams M, Bever AJ, Foresman E. 2016. 3-D simulations of the San Francisco Estuary with subgrid bathymetry to explore long-term trends in salinity distribution and fish abundance. San Franc. Estuary Watershed Sci. [accessed 2020 Dec 10];14(2). *https://doi.org/10.15447/sfews.2016v14iss2art3*

MacWilliams ML, Bever AJ, Gross ES, Ketefian GS, Kimmerer WJ. 2015. Three-dimensional modeling of hydrodynamics and salinity in the San Francisco Estuary: an evaluation of model accuracy, X2, and the low salinity zone. San Franc. Estuary Watershed Sci. [accessed 2021 Mar 17];13(1). *https://doi.org/10.15447/sfews.2015v13iss1art2*

MacWilliams ML, Cheng RT, 2007. Three-dimensional hydrodynamic modeling of San Pablo Bay on an unstructured grid. 7th International Conference on Hydroscience and Engineering (Philadelphia, Pennsylvania); September 2007.

MacWilliams ML, Gross ES. 2007. UnTRIM San Francisco Bay–Delta Model Calibration Report, Delta Risk Management Study. Prepared for the California Department of Water Resources. March 2007.

MacWilliams ML, Gross ES. 2013. Hydrodynamic simulation of circulation and residence time in Clifton Court Forebay. San Franc. Estuary Watershed Sci. [accessed 2020 Dec 10];11(2). *https://doi.org/10.15447/sfews.2013v11iss2art1*

MacWilliams ML, Salcedo FG, Gross ES. 2008. San Francisco Bay–Delta UnTRIM model calibration report, POD 3-D particle tracking modeling study. Prepared for the California Department of Water Resources. [accessed 2008 Dec 19].

MacWilliams ML, Salcedo FG, Gross ES. 2009. San Francisco Bay–Delta UnTRIM model calibration report, Sacramento and Stockton deep water ship channel 3-D hydrodynamic and salinity modeling study. Prepared for the US Army Corps of Engineers, San Francisco District. 14 July 2009.

McEwan DR. 2001. Central Valley Steelhead. In: Brown RL, editor. 2001. Contributions to the biology of Central Valley salmonids. Volume 1. Fish Bulletin 179. [accessed 2022 Mar 29]. Sacramento (CA): California Dept. of Fish and Game. Available from: *https://escholarship.org/uc/item/6sd4z5b2*

Michel CJ, Smith JM, Demetras NJ, Huff DD, Hayes SA. 2018. Non-native fish predator density and molecular-based diet estimates suggest differing impacts of predator species on juvenile salmon in the San Joaquin River, California. San Franc. Estuary Watershed Sci. [2022 Dec 15];16(4). *https://doi.org/10.15447/sfews.2018v16iss4art3*

Newman KB. 2003. Modelling paired release–recovery data in the presence of survival and capture heterogeneity with application to marked juvenile salmon. Stat Model. [accessed 2015 May 28];3:157–177. *https://doi.org/10.1191/1471082X03st055oa*

Nichols FH, Cloern JE, Luoma SN, Peterson DH. 1986. The modification of an estuary. Science. [accessed 2021 Feb 2];231:567–573. *https://doi.org/10.1126/science.231.4738.567*

[NMFS] National Marine Fisheries Service. 2009. Endangered Species Act Section 7 consultation: Biological opinion and conference opinion on the long-term operations of the Central Valley Project and State Water Project. NMFS, Southwest Region, Long Beach, California. June 4, 2009; amended April 7, 2011.

[NOAA] National Oceanic and Atmospheric Administration. 2025a. Environmental Research Divisions Data Access Program. [accessed 2024 January 2024]; Available from: *https://oceanview.pfeg.noaa.gov/erddap/index.html*

[NOAA] National Oceanic and Atmospheric Administration. 2025b. Environmental Research Divisions Data Access Program: Environmental Research Divisions Projects. [accessed 2024 January 2024]. Available from: *https://oceanview.pfeg.noaa.gov/erddap/search/index.html?page=1&itemsPerPage=1000&searchFor=FEDSDFRCS*

Nobriga ML, Michel CJ, Johnson RC, Wikert JD. 2021. Coldwater fish in a warm water world: implications for predation of salmon smolts during estuary transit. Ecol Evol. [accessed 2022 May 20];11(15):10381–10395. *https://doi.org/10.1002/ece3.7840*

Perry RW, Skalski JR, Brandes PL, Sandstrom PT, Klimley AP, Ammann A, MacFarlane B. 2010. Estimating survival and migration route probabilities of juvenile Chinook Salmon in the Sacramento–San Joaquin River Delta. N Am J Fish Manag. [accessed 2021 Nov 9];30(1)142–156. *https://doi.org/10.1577/M08-200.1*

Perry RW, Brandes PL, Burau JR, Klimley AP, MacFarlane B, Michel C, Skalski JR. 2013. Sensitivity of survival to migration routes used by juvenile Chinook Salmon to negotiate the Sacramento–San Joaquin River Delta. Environ Biol Fishes. [accessed 2022 Mar 17];96:381–392. *https://doi.org/10.1007/s10641-012-9984-6*

[PFMC] Pacific Fishery Management Council. 2023. Amended review of 2023 ocean salmon fisheries stock assessment and fishery evaluation document for the Pacific Coast Salmon Fishery Management Plan. February 2024; amended April 2024. [accessed 2024 Oct 10]. Available from: *https://www.pcouncil.org/documents/2024/02/review-of-2023-ocean-salmon-fisheries.pdf/*

https://doi.org/10.15447/sfews.2026v24iss3art4

R Core Team. 2021. R: A language and environment for statistical computing. Vienna (Austria): R Foundation for Statistical Computing.

[SJRGA] San Joaquin River Group Authority. 2011. 2010 Annual Technical Report. On Implementation and Monitoring of the San Joaquin River Agreement and the Vernalis Adaptive Management Plan. Prepared for the California Water Resources Control Board in compliance with D-1641. August 2011. [accessed 2024 Sep 9]. 167 p. Available from: *http://tuolumnerivertac.com/Documents/SJRGA2011_2010AnnualTechnicalReport.pdf*

[SJRGA] San Joaquin River Group Authority. 2013. 2011 Annual Technical Report. San Joaquin River Agreement, Vernalis Adaptive Management Plan. On implementation and monitoring of the San Joaquin River Agreement and the Vernalis Adaptive Management Plan (VAMP). Prepared for the California Water Resources Control Board in compliance with D-1641. February 2013. [accessed 2024 Sep 9]. 339 p. Available from: *http://tuolumnerivertac.com/Documents/SJRGA2013_2011AnnualTechnicalReport_compressed.pdf*

Smith CD, Plumb JM, Adams NS, Wyatt, GJ. 2021. Predator and prey events at the entrance of a surface-oriented fish collector at North Fork Dam, Oregon. Fish Manag Ecol. [accessed 2022 Mar 16];28(2):172–182. *https://doi.org/10.1111/fme.12465*

Sokal RR, Rohlf FJ. 1995. Biometry. (3rd ed.) New York (NY): Freeman. 887 p.

[SST] Salmonid Scoping Team. 2017a. Effects of water project operations on juvenile salmonid migration and survival in the South Delta. Findings and Recommendations. Volume I. Sacramento (CA): Collaborative Adaptive Management Team (CAMT) SST. 111 p.

[SST] Salmonid Scoping Team. 2017b. Effects of water project operations on juvenile salmonid migration and survival in the South Delta. Findings and Recommendations. Volume II. Sacramento (CA): Collaborative Adaptive Management Team (CAMT) SST. 60 p.

Thieurmel B, Elmarhraoui A. 2022. 'suncalc': compute sun position, sunlight phases, moon position and lunar phase. R package version 0.5.1. Available from: *https://CRAN.R-project.org/package=suncalc*

Towne K, Brandes P, Nichols K, Buchanan R, Ammann A, Singer G, Chapman E. 2022. 2017 South Delta Chinook Salmon survival study: Draft Report. Brandes P, Castillo G, editors. 20 April 2022. [accessed 2022 Apr 20]. Available from: *https://www.researchgate.net/publication/360074367_2017_South_Delta_Chinook_Salmon_Tagging_Study_DRAFT_REPORT*

Vogel DA. 2011. Evaluation of acoustic-tagged juvenile Chinooks and predatory fish movements in the Sacramento–San Joaquin Delta during the 2010 Vernalis Adaptive Management Program. Red Bluff (CA): Natural Resource Scientists, Inc. [accessed 2025 Se 24]. Available from: *https://filelib.wildlife.ca.gov/Public/Adult_Sturgeon_and_Striped_Bass/Staff%20Report%20---%20Literature%20Cited/Vogel%202011.pdf*

Wang X, Perry RW, Pope AC, Jackson D. 2024. Individual-based ecological particle tracking model (ECO-PTM) for simulating juvenile Chinook Salmon migration and survival through the Sacramento–San Joaquin Delta. San Franc. Estuary Watershed Sci. [accessed 2025 Jan 31];22(4). *https://doi.org/10.15447/sfews.2024v22iss4art4*

Williams JG. 2006. Central Valley salmon: a perspective on Chinook and steelhead in the Central Valley of California. San Franc Estuary Watershed Sci. [accessed 2024 Oct 10];4(3). *https://doi.org/10.15447/sfews.2006v4iss3art2*

Williamson KS, May B. 2005. Homogenization of fall-run Chinook Salmon gene pools in the Central Valley of California, USA. N Am J Fish Manag. [accessed 2024 Oct 10];25:993–1009. *https://doi.org/10.1577/M04-136.1*

Wohner PJ, Duarte A, Wikert J, Cavallo B, Zeug SC, Peterson JT. 2022. Integrating monitoring and optimization modeling to inform flow decisions for Chinook Salmon smolts. Ecol Model. [accessed 2023 Sep 14];471:110058. *https://doi.org/10.1016/j.ecolmodel.2022.110058*

Yoshiyama RM, Moyle PB, Gerstung ER, Fisher FW. 2000. Chinook Salmon in the California Central Valley: an assessment. Fisheries. [accessed 2024 Oct 10];25(2):6–20. *https://doi.org/10.1577/1548-8446(2000)025%3C0006:CSITCC%3E2.0.CO;2*